nature communications

Article

https://doi.org/10.1038/s41467-026-71328-9

A single-nucleotide enhancer mutation overrides chromosomal sex to drive XX male development

Received: 9 September 2025

Accepted: 17 March 2026

Published online: 09 April 2026

Check for updates

Elisheva Abberbock[1], Meshi Ridnik[1], Isabelle Stévant[1], Roni Weiss[1], Carmel Bamberger[1], Shelly Ziv Lhermann[1], Maor Lubman[1], Yumi Minyi Yao[2], Ariel Afek[2], Francis Poulat[3] & Nitzan Gonen[1]

Mammalian sex determination is governed by two mutually antagonistic genetic programs that must be precisely balanced. Activation of *Sox9* initiates testis development, while its repression is essential for ovarian fate. The distal enhancer, Enh13, is essential for testicular *Sox9* expression, with its deletion or inactivation resulting in complete XY sex reversal. Here, we show that subtle mutations within Enh13, including a single-nucleotide insertion, produce the reciprocal phenotype: complete XX female-to-male sex reversal. Pro-female factors can strongly repress Enh13, suggesting they mediate *Sox9* silencing in ovaries. The small enhancer alterations facilitate inappropriate *Sox9* upregulation in the absence of *Sry*, triggering the testicular transcriptome and repressing ovarian gene expression. Mechanistically, these mutations disrupt the repressive effect of RUNX1, NR5A1 and GATA4, thereby reprogramming enhancer activity. Our findings identify Enh13 as a central regulatory hub, integrating opposing sex-specific cues, hence acting as a binary switch for gonadal fate.

In eutherian mammals, the sex of the individuals is established through a succession of events that eventually provide them with functional reproductive organs. First, genetic sex is defined at fertilization by the provision of an X or a Y chromosome by the sperm to an X-bearing oocyte. Later, during gestation, the undifferentiated bipotential gonad adopts a testicular or ovarian fate upon a process called gonadal sex determination[1–3]. Once differentiated, the gonads produce sex hormones necessary for the development of internal and external genitalia, secondary sexual characteristics, and then control puberty and fertility of the individual[4].

Gonadal sex determination is mediated by two antagonistic genetic programs involving the activation of pro-male or pro-female factors, but also the silencing of the alternative sex genes. Testis development is initiated by the activity of the *Sry* gene, located on the Y chromosome, which activates its downstream autosomal target gene, *Sox9*[5–8]. SOX9, the master regulator of Sertoli cell differentiation and testis development, drives the transcription of downstream target genes critical for testis formation[5,8–10]. Indeed, human individuals and mice with mutations in *SRY* or *SOX9* are born as XY females[8,11–15]. On the contrary, forced expression of *SOX9* in both human individuals and mice drives testis differentiation of XX gonads[16–19]. Ovary development relies on the activity of several pro-female factors, including the WT1(-KTS) isoform[20], WNT4/RSPO1/β-CATENIN[21–25], FOXL2[26–28] and RUNX1[29]. Knockouts (KOs) of individual pro-female factors result in only partial XX sex reversal, while double KOs of either *Runx1*, *Rspo1* or *Wnt4* together with *Foxl2* amplify the XX female-to-male sex reversal phenotype[29–32], suggesting a redundant function of the pro-female factors during ovarian development. It is proposed that repression of *Sox9* expression is required for proper ovary development, yet the molecular mechanisms remain largely unknown[33].

[1]The Mina and Everard Goodman Faculty of Life Sciences and the Institute of Nanotechnology and Advanced Materials, Bar-Ilan University, Ramat Gan, Israel. [2]Department of Chemical and Structural Biology, Weizmann Institute of Science, Rehovot, Israel. [3]Group "Development and Pathology of the Gonad". Department of Genetics and Development, IGH, University of Montpellier, CNRS, Montpellier, France. e-mail: nitzan.gonen@biu.ac.il

We have previously identified Enhancer 13 (Enh13) as the critical regulator of the *Sox9* gene in the testis[34]. Enh13 is a 557 bp-long enhancer, located 565 kb upstream of the *Sox9* gene. Deletion of Enh13 in both mice and humans leads to XY male-to-female sex reversal[34,35]. Upon Enh13 deletion, *Sox9* expression level drops by 80%, leading to ovarian development despite the presence of a Y chromosome, the *Sry* gene, and two intact *Sox9* copies[34]. Furthermore, we have recently shown that mutating together the SOX9 and SRY transcription factor binding sites (TFBS) within Enh13 is enough to induce XY female development in vivo[36]. While the role of Enh13 in activating testis development is now well established, our results did not suggest it may also have a function during ovarian development[34,36]. However, several XX patients with Differences of Sex Development (DSD) (46, XX DSD) were identified carrying a ~3.7-5 kb duplication that includes the human Enh13 (also called eSR-A)[37,38], suggesting that having an additional Enh13 copy may lead to *SOX9* expression and testis development in the absence of SRY.

Here, we show that XX mice carrying a 3 bp deletion or a 1 bp insertion within the SOX9 binding site (BS) of Enh13 present with female-to-male sex reversal. Adult XX mice appear externally and internally as males, but with small testes devoid of sperm due to the lack of the Y chromosome[6,39]. At embryonic stages, XX homozygous gonads appear as ovotestis to different extents across individuals and depending on the mutation, with the 1 bp insertion appearing more like a testis compared to the 3 bp deletion. Transcriptomic analysis of E12.5 gonads shows that indeed XX homozygous gonads express both the testicular and ovarian genes, while XY homozygous gonads are indistinguishable from *wild type* (WT) XY gonads. TFBS analysis suggests that Enh13 contains binding sites for pro-female factors and that the SOX9 BS overlaps with a RUNX1 BS. Indeed, reporter assays indicate that Enh13 can be repressed by RUNX1 and other pro-female factors. Delving into the mechanism exerted by the 3 bp deletion and 1 bp insertion XX mutants, we show that the mutations do not abolish SOX9 binding but rather prevent repression by the bipotential factors NR5A1, GATA4, and RUNX1 to allow sufficient activating capacity to induce *Sox9* expression above the minimal threshold present in the female gonad. Once expressed, SOX9 further enhances its own expression and drives testis development in XX individuals. These findings implicate Enh13 as a regulatory element essential for both testicular and ovarian development, placing it at the critical junction of sexual differentiation pathways. This also highlights that even small changes within regulatory elements can induce dramatic phenotypic outcomes.

Results

Small mutations in the SOX9 BS of Enh13 lead to XX male development in adulthood

In our previous study aiming to identify the functional elements of Enh13, we have generated mice carrying mutations in several TFBS, including NR5A1, SOX9 and SRY[36]. Using CRISPR-Cas9, we obtained two different mouse strains with mutations within the SOX9 BS, one with a 20 bp deletion that completely abolished the SOX9 BS (Supplementary Fig. 1A, termed Enh13$^{SOX9*-20bp}$) and one with a 3 bp deletion that removed 3 nucleotides at the center of the SOX9 BS (Fig. 1A, termed Enh13$^{SOX9*-3bp}$). When looking at the sequence of the Enh13$^{SOX9*-3bp}$, we noticed that we recreated a quasi-identical SOX9 BS (CACAATGG, Fig. 1A, B), so we did not consider using this strain in our previous study. Heterozygous and homozygous XX and XY Enh13$^{SOX9*-20bp}$ mice presented normal phenotypes, i.e., XX females with ovaries, and XY males with testes, demonstrating that the SOX9 BS alone is not responsible for the Enh13 activity (Supplementary Fig. 1B-C), but instead acts redundantly with the SRY BS to control the *Sox9* gene expression[36]. While XX and XY heterozygous and XY homozygous mice carrying the Enh13$^{SOX9*-3bp}$ also presented normal phenotypes (Supplementary Fig. 2A, B), XX mice homozygous for the 3 bp deletion were born sex reversed highlighted by male external genitalia and small testes (Fig. 1C). Immunostaining of adult gonads with markers of Sertoli cells of the testis (SOX9), granulosa cells of the ovary (FOXL2) and gonocytes (DDX4) revealed that XX Enh13$^{SOX9*-3bp-/-}$ homozygous gonads show no FOXL2 expression and instead contain seminiferous tubules, marked by SOX9 expression. These seminiferous tubules lack DDX4-positive gonocytes at 6-week-old mice (Fig. 1D), a phenotype known to occur in XX males as they are not able to support spermatogenesis in the absence of Y chromosome genes[6,39].

To better characterise the phenotype, we explored the expression levels of *Sox9*, *Sox8*, a downstream target gene of SOX9 in Sertoli cells[14], and *Foxl2* in adult gonads. XX WT and heterozygous gonads exhibited low expression of *Sox9* and *Sox8* while having high *Foxl2* expression (Fig. 1E). XY WT gonads had high expression of *Sox9* and *Sox8* and no detectable *Foxl2* expression. XX homozygous gonads for the 3 bp deletion were similar to XY WT gonads, with high expression levels of *Sox9* and *Sox8* and no detectable *Foxl2* expression, confirming a female-to-male sex reversal in adulthood (Fig. 1E).

Early E10.5 gonads of XY and XX both express low levels of (cytoplasmic) SOX9, after which *Sox9* is highly upregulated in the testes and decreased in ovaries[40,41]. In XY gonads, SRY induces *Sox9* expression by binding to Enh13, and subsequently, SOX9 controls its own expression by binding to both the SOX9 and SRY BSs of Enh13[36]. Since SOX9 protein can bind to both SRY and SOX9 TFBS, we tested whether the elevated *Sox9* expression observed in the XX Enh13$^{SOX9*-3bp-/-}$ is due to SOX9 binding to both the mutated SOX9 BS as well as the SRY BS. To that aim, we generated mice carrying the same 3 bp deletion in the SOX9 BS along with a deletion removing the entire SRY BS (Supplementary Fig. 3A, termed Enh13$^{SOX9*-3bp\ SRY*-12bp}$). Heterozygous and homozygous XY mice developed as males, while XX heterozygous mice presented as female mice (Supplementary Fig. 3B, C). Homozygous XX mice presented as males (Supplementary Fig. 3B, C), demonstrating that removal of the SRY BS, to which SOX9 can bind, does not affect the female-to-male sex reversal phenotype, suggesting that the mutated SOX9 BS is still functional and able to induce *Sox9* expression. These results denote that, in this sensitized context, the loss of the SRY BS does not prevent testis development in XY. The 3 bp deletion alone allows *Sox9* expression to rise above the critical level required to trigger testicular differentiation in XX and XY gonads. Moreover, the female-to-male sex reversal is solely due to the 3 bp deletion and does not involve the SRY motif, to which SOX9 can bind.

We next wanted to examine whether other insertion/deletions (INDELs) within the SOX9 BS of Enh13 will cause a similar phenotype. To that aim, we generated a mouse strain carrying 1 bp insertion in the SOX9 BS (Fig. 1F, termed Enh13$^{SOX9*+1bp}$). Heterozygous XX mice presented as females while heterozygous and homozygous XY mice presented as males (Supplementary Fig. 3D). Similarly to what we observed with the 3 bp deletion, XX homozygous mice carrying only a 1 bp insertion in Enh13 were born as XX males with small testes (Fig. 1G). Immunostaining of adult gonads confirmed complete sex reversal and the presence of seminiferous tubules lacking gonocytes (Supplementary Fig. 3E). Altogether, these findings underscore the extraordinary sensitivity of the *Sox9* regulatory network to subtle enhancer perturbations, showing that specific mutations are capable of inducing *Sox9* expression above a critical threshold required to initiate testicular development in an XX context.

Embryonic gonads develop as ovotestis upon small mutations in the SOX9 BS of Enh13

We then sought to explore whether the sex reversal observed in XX adult gonads occurs during early gonadal development. We hence collected E13.5 gonads from XX and XY WT as well as XX Enh13$^{SOX9*-3bp-/-}$ embryos. XX gonads of Enh13$^{SOX9*-3bp-/-}$ embryos presented variable phenotypes of ovotestis. At E13.5, WT testes are organised into testis cords, containing Sertoli cells and germ cells, along with an interstitial

https://doi.org/10.1038/s41467-026-71328-9

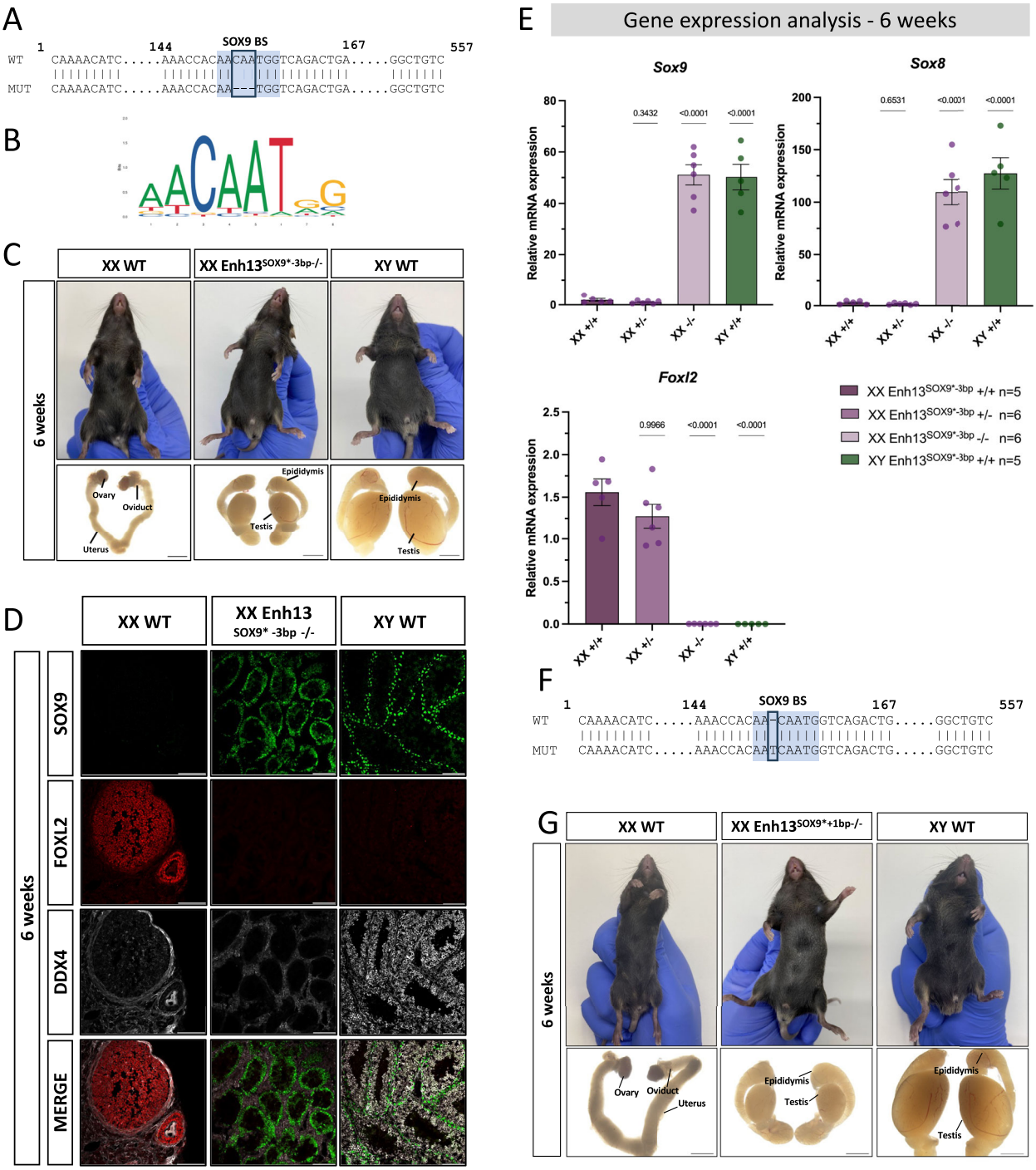

Fig. 1 | Small mutations in the SOX9 BS of Enh13 lead to XX male development in adults. A–E Characterization of mouse strain containing a 3bp deletion in the SOX9 BS of Enh13 (Enh13 $^{SOX9*-3bp}$). **F, G** Characterization of mouse strain containing a 1bp insertion in the SOX9 BS of Enh13 (Enh13 $^{SOX9*+1bp}$). **A, F** Sequence representation alignment between the WT sequence and the homozygous mutation of each mouse line using the online alignment tool - BLAST. SOX9 BS is highlighted in blue. **B** SOX9 binding motif (JASPAR ID: MA0077.2) taken from the JASPAR database. **C, G** Bright field images of the external and internal genitalia and gonads of 6-week-old adult male (XY) and female (XX) WT mice, and XX homozygous mice from each mouse line. Scale bar represents 2000 μm (**D**) Immunostaining of 6-week-old gonads from XY WT, XX Enh13 $^{SOX9*-3bp-/-}$ and XX WT. Gonads were stained for Sertoli-marker SOX9 (green), granulosa-marker FOXL2 (red) and germ cell marker DDX4 (grey). Scale bars represent 100 μm. This experiment was repeated 6 times independently with similar results. **E** Real-time quantitative PCR analysis of genes involved in male (*Sox9* and *Sox8*) and in female (*Foxl2*) gonadal development in 6-week-old gonads. Data are presented as mean $2^{-\Delta\Delta Ct}$ values, normalized to the housekeeping gene *Hprt*. Sample size is indicated on the graph, where each dot represents an individual mouse. Error bars show SEM of $2^{-\Delta\Delta Ct}$ values. Statistical analysis was done by one-way ANOVA followed by Dunnett's posttest. All samples were compared to the XX WT. $^{*}P < 0.05$, $^{**}P < 0.01$, $^{***}P < 0.001$, and $^{****}P < 0.0001$, ns- not significant. WT- *Wild Type*. Source data are provided as a Source Data file.

compartment where Leydig cells reside, and present with a coelomic vessel. WT ovaries, on the other hand, are devoid of clear structural organisation at that stage and germ cells along with somatic cells are spread across the ovarian area. While some XX homozygous gonads appeared mostly as testes with coelomic vessel and testis cords, others had a coelomic vessel without clear testis cords and some presented with a testicular gonadal portion alongside an ovarian portion (Fig. 2A). Variability in ovotestis phenotypes were also evident between the right and left gonads of the same embryo where in one the anterior portion was ovarian and the posterior was testicular, whereas the other gonad presented an anterior and posterior ovarian portions and a centralised testicular portion (Fig. 2A, first and third mutant gonads are the left and right gonads of the same embryo). It is important to note that all embryos are on the same C57BL6/J genetic background, and hence the variable phenotype does not stem from differences in genetic background as reported in other cases[42]. Notably, XX heterozygous gonads were indistinguishable from XX WT gonads (Supplementary Fig. 4A) while XY heterozygous and homozygous gonads were indistinguishable from XY WT gonads (Supplementary Fig. 4B).

To better explore this ovotestis phenotype, we performed immunostaining on E13.5 embryonic gonads using SOX9, FOXL2 and TRA98 (marks gonocytes). XX Enh13$^{SOX9^{*}-3bp-/-}$ gonads presented with ovotestis with an anterior ovarian portion alongside a testicular posterior portion, or an ovotestis where the testicular tissue is centrally located, flanked by ovarian domains at both poles (Fig. 2B). FOXL2 and SOX9 positive cells were mutually exclusive (Fig. 2B, larger magnification). Immunostaining of XX heterozygous gonads (Supplementary Fig. 4C) or XY heterozygous and homozygous gonads (Supplementary Fig. 4D) demonstrated they are similar to XX WT or XY WT, respectively.

To confirm the ovotestis phenotype, we measured the expression levels of *Sox9*, *Sox8* and *Foxl2* by qPCR at E13.5. Overall, *Sox9* levels in XX homozygous gonads are comparable to WT XY gonads, though sample variability likely reflected differences in the extent of ovotestis phenotype (Fig. 2C). Heterozygous XX gonads had similar expression levels to XX WT controls (Fig. 2C). *Sox8* and *Foxl2* expression in homozygous XX gonads presented an intermediate level of expression compared to the XX WT and XY WT gonads, consistent with a mixed gonadal identity.

Whereas XX individuals from the three mutant mouse lines: Enh13$^{SOX9^{*}-3bp-/-}$, Enh13$^{SOX9^{*}+1bp-/-}$ and Enh13$^{SOX9^{*}-3bp\ SRY^{*}-12bp-/-}$ showed complete XX female-to-male sex reversal in adulthood, we wanted to explore whether they all present with an ovotestis phenotype at embryonic stages. To that aim, we examined E13.5 gonads from the Enh13$^{SOX9^{*}+1bp-/-}$ and Enh13$^{SOX9^{*}-3bp\ SRY^{*}-12bp-/-}$ by both bright field (Supplementary Fig. 4E-F) and immunostaining (Fig. 2D, Supplementary Fig. 4G). XX homozygous mutant gonads from the Enh13$^{SOX9^{*}+1bp-/-}$ (Fig. 2D) and Enh13$^{SOX9^{*}-3bp\ SRY^{*}-12bp-/-}$ (Supplementary Fig. 4G) strains also presented an ovotestis phenotype, with a more testis-like appearance compared to the Enh13$^{SOX9^{*}-3bp-/-}$ strain. Gonads displayed SOX9 expression along with a very limited FOXL2-positive region, typically restricted to one or two poles of the gonad (Fig. 2D, Supplementary Fig. 4G).

Since E13.5 mutant gonads presented as ovotestes to different extents, and at 6 weeks, these gonads were testis expressing SOX9, but no FOXL2, this prompted us to explore mutant gonads also at two intermediate time points: E15.5 and P1 (Supplementary Fig. 5). Bright field analysis confirmed that E15.5 and P1 gonads from both mutants (Enh13$^{SOX9^{*}+1bp-/-}$ and Enh13$^{SOX9^{*}-3bp-/-}$) presented as a testis (Supplementary Fig. 5A, D). Immunostaining at E15.5 showed that FOXL2 is still expressed in either just the anterior pole or both poles, much more so in the Enh13$^{SOX9^{*}-3bp}$ mutants rather than the Enh13$^{SOX9^{*}+1bp}$ mutants (Supplementary Fig. 5B, C). Analysis of mutant gonads at P1 presented mostly SOX9-positive cells with very few FOXL2-positive cells, located mostly in the cortex, more in the Enh13$^{SOX9^{*}-3bp}$ mutants rather than the Enh13$^{SOX9^{*}+1bp}$ mutants (Supplementary Fig. 5E, F). Altogether, these analyses indicate that the Enh13$^{SOX9^{*}+1bp}$ mutant appears to have a stronger ability for sex reversal than the Enh13$^{SOX9^{*}-3bp}$ mutant, as more FOXL2-positive cells persist postnatally at P1 in the Enh13$^{SOX9^{*}-3bp}$ mutant.

Transcriptomic analysis of E12.5 embryonic gonads demonstrates an ovotestis pattern

To gain insight into the molecular and transcriptomic consequences of small mutations within Enh13, and to determine whether different INDEL alleles elicit distinct gene expression profiles, we performed RNA-seq on E12.5 embryonic gonads. We chose the E12.5 stage as it is known that ovarian development is lagged ~1 day behind compared to testis differentiation that commences at E11.5[20,43]. Therefore, analysing E12.5 gonads seemed to be an optimal stage to capture the early transcriptomic changes that eventually lead to ovotestis, followed by testis development. Pairs of E12.5 gonads from individual embryos were harvested and bulk RNA-seq was performed. We harvested 3 pairs of gonads from XX and XY WT and heterozygous embryos, while we collected 5 gonads from XY and XX homozygous embryos for the 3 different mutant mouse strains (Enh13$^{SOX9^{*}-3bp}$, Enh13$^{SOX9^{*}+1bp}$ and Enh13$^{SOX9^{*}-3bp\ SRY^{*}-12bp}$) as we assumed there may be a higher degree of variability there. Principal component analysis (PCA) demonstrated that XX WT and heterozygous gonads mostly clustered together (Fig. 3A). XY WT, heterozygous and homozygous gonads also clustered together, suggesting that the small mutations do not hamper testis development in the context of XY. PC1, which accounts for 27.7% of the variability, clearly separated the testis (right side) and the ovary (left side) (Fig. 3A). The XX homozygous gonads were positioned between the testis and the ovary, and a large degree of variability was evident between the three different mutant mouse strains and even between the samples of each strain. Spearman pairwise sample correlation analysis supported these findings and separated the XX homozygous samples from both the XX ovaries and XY testis (Supplementary Fig. 6A).

We next performed differential expression analysis on all samples to identify early genes driving the gonadal sex change (Fig. 3B, Supplementary Data 1). 1,803 genes were found to be differentially expressed and could be classified into 6 groups (*a* to *f*) based on their expression profile. Groups *a-c* exhibited genes with increased expression in the ovary, while groups *e-f* constitute genes with increased expression in the testis. Consistent with the ovotestis phenotype, the XX homozygous gonads presented a transcriptomic profile that is different from the testicular and ovarian ones, with expression of both testicular and ovarian genes together, albeit at lower levels (Fig. 3B).

We then examined the expression profile of specific genes associated with various cell types of the gonads. Analysis of bipotential genes, *Gata4* and *Zfpm2* (*Fog2*), which are expressed in supporting cell precursors, and later maintained in both Sertoli and pre-granulosa cells, revealed no major differences in expression between WT, heterozygous, and homozygous gonads from the Enh13$^{SOX9^{*}-3bp}$, Enh13$^{SOX9^{*}+1bp}$ and Enh13$^{SOX9^{*}-3bp\ SRY^{*}-12bp}$ mutants (Supplementary Fig. 7A). *Nr5a1* expression in the XX homozygous mutants was more similar to the male expression levels, whereas *Wt1* expression in the homozygous mutants resembles more that of the WT XX gonads (Supplementary Fig. 7A). Markers expressed in pre-granulosa cells as *Foxl2*, *Fst*, *Bmp2*, *Wnt4*, *Runx1*, *Rspo1*, *Lhx9* and *Emx2* were highly expressed in XX WT and XX heterozygous gonads, but displayed a low-to-intermediate expression in the XX homozygous mutant gonads of the 3 mouse strains (Fig. 3C and Supplementary Fig. 7B). A mirrored expression pattern was observed for Sertoli cell markers, including *Sox9*, *Sox8*, *Fgf9*, *Dhh*, *Amh, Gdnf* and *Aard*. These genes were highly expressed in XY WT, heterozygous, and homozygous gonads, absent in XX WT and heterozygous gonads, but displayed intermediate to high expression in all XX homozygous mutant

https://doi.org/10.1038/s41467-026-71328-9

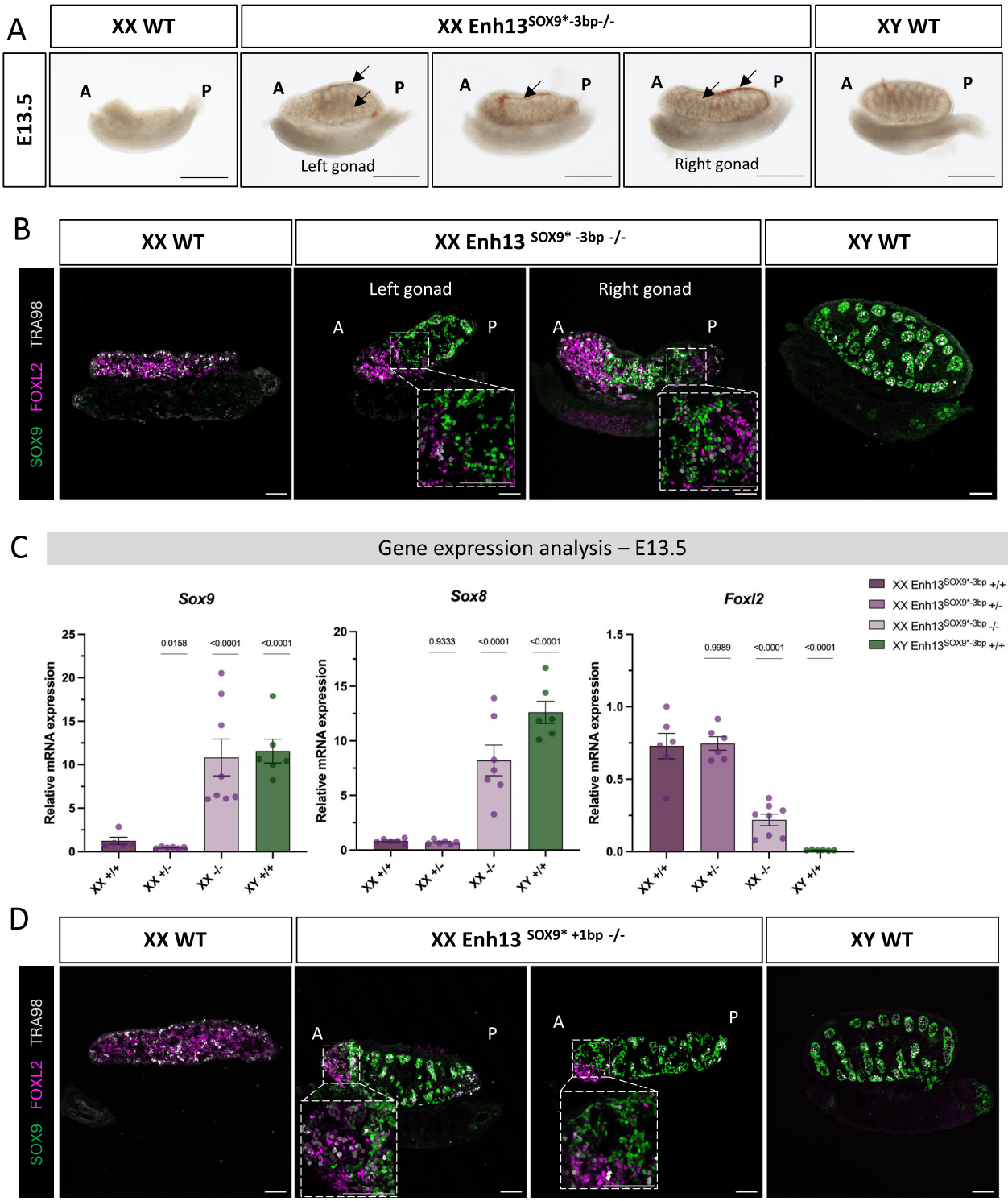

Fig. 2 | Small mutations in the SOX9 BS of Enh13 lead to ovotestis gonad development at embryonic stages. Characterization of E13.5 gonads from the Enh13 $^{SOX9*-3bp-/-}$ (**A**–**C**) and Enh13 $^{SOX9*+1bp-/-}$ (**D**) mouse lines. **A** Bright field images of E13.5 gonads of XX WT, XY WT and XX Enh13 $^{SOX9*-3bp-/-}$ mice. Scale Bar represents 500 μm. Arrows pointing to the coelomic vessels and testis cords. From left to right, the first and third gonads of the XX homozygous mice are from the same embryo. A-anterior, P-posterior. This experiment was repeated 15 times independently with similar results. **B**, **D** Immunostaining of E13.5 gonads from XY and XX WT as well as XX homozygous mice from each mouse line. Gonads were stained for Sertoli-marker SOX9 (green), granulosa-marker FOXL2 (magenta) and germ cell marker TRA98 (grey). Scale Bar represents 100 μm. XX homozygous gonads in B are the right and left gonads dissected from the same embryo. These experiment was repeated 6 times independently with similar results. **C** Real-time quantitative PCR analysis of genes involved in male (*Sox9* and *Sox8*) and in female (*Foxl2*) gonadal sex determination in E13.5 gonads. Data are presented as mean $2^{-\Delta\Delta Ct}$ values, normalized to the housekeeping gene *Hprt*. The sample size is indicated on the graph, where each dot represents an individual embryo. Error bars show SEM of $2^{-\Delta\Delta Ct}$ values. Statistical analysis was done by one-way ANOVA followed by Dunnett's posttest. All samples are compared to the XX WT. $^{*}P < 0.05$, $^{**}P < 0.01$, $^{***}P < 0.001$, and $^{****}P < 0.0001$, ns- not significant. WT- *Wild Type*. Source data are provided as a Source Data file.

https://doi.org/10.1038/s41467-026-71328-9

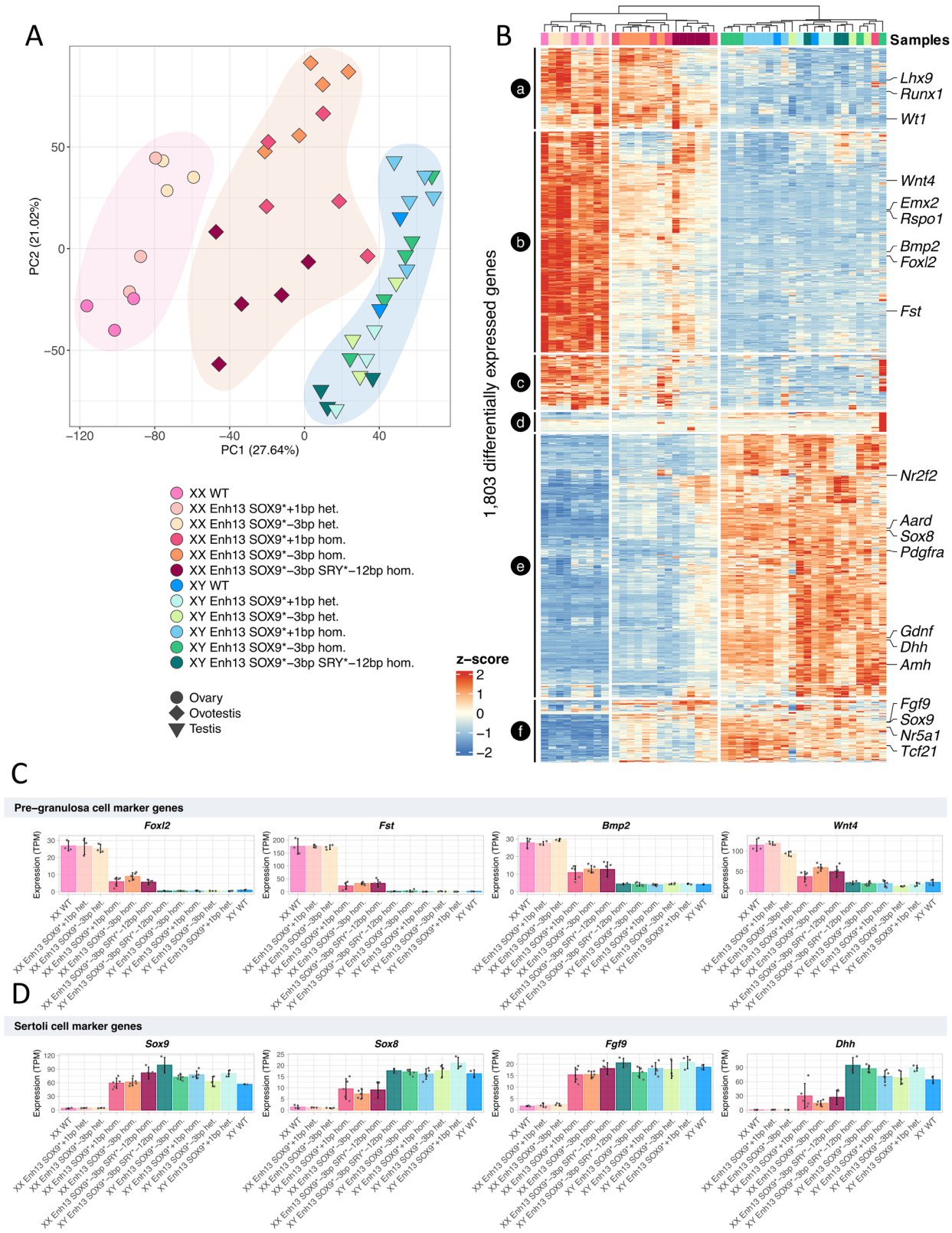

gonads (Fig. 3D and Supplementary Fig. 7C). Notably, *Sox9* and *Fgf9* showed the highest expression levels, whereas the remaining markers exhibited intermediate expression, likely reflecting their later activation during testis development, as E12.5 precedes their peak expression[44–46]. Examination of markers of germ cells and interstitial/stromal cells did not exhibit any dramatic change between all samples (Supplementary Fig. 7D, E).

Altogether, this transcriptomic analysis, at an early stage of the sex reversal process, reveals that transcriptomes of heterozygous XY and XX gonads, as well as homozygous XY gonads, are indistinguishable from their respective WT counterparts. In contrast, XX homozygous gonads from all three mutant strains exhibit a mixed ovarian and testicular transcriptome signature at E12.5.

Fig. 3 | Transcriptomic analysis of E12.5 embryonic gonads reveals an ovotestis state. A PCA of the transcriptomes from E12.5 XX and XY whole gonads of WT ($n = 3$) and mutant heterozygous ($n = 3$) and homozygous ($n = 5$) embryos. Each point represents the transcriptome of a pair of gonads, separated from the mesonephros. Samples are coloured by their genotype, and the shape of the point represents the phenotype of the gonads (circle- ovary, triangle- testis, diamond- ovotestis). **B** Heatmap representing the differentially expressed genes between the samples. Expression data were normalized as Z-scores. Differentially expressed genes were clustered into 6 groups labelled from *a* to *f* as indicated on the left-hand side of the heatmap. Samples were grouped using unsupervised clustering as represented by the dendrogram at the top of the heatmap. Names of well-known gonadal marker genes are indicated on the left-hand side. Expression profiles of well-known gonadal marker genes for pre-granulosa cells (**C**) and Sertoli cells (**D**). Expression values are expressed as TPM (Transcript per million), the bars represent the median of expression, and each point represents a single biological replicate. Error bars represent the standard deviation across the replicates. WT- *Wild Type*.

The SOX9 BS mutations do not abolish the ability of SOX9 to bind and activate Enh13

We next wanted to explore the molecular mechanisms leading to these small mutations, in an XX environment, to enable activation of *Sox9* expression, driving testis development. As the mutations lie within the SOX9 binding site, and since it still appears to be a putative SOX9 BS, even in the presence of the mutations (Fig. 1B), we hypothesised that these mutations might enhance SOX9 binding and promote activation, given its low-level cytoplasmic expression in XX gonads before sex determination[40,47]. To test this, we performed Protein Binding Microarray (PBM)[48] and electro mobility shift assays (EMSA) with in vitro–translated SOX9 on synthetic Enh13 sequences (WT, −3 bp, +1 bp). Both assays confirmed SOX9 binding, albeit with lower affinity, with even further reduced affinity in the 3 bp deletion mutant (Supplementary Fig. 8A–C). Luciferase assays in HEK293T cells supported this, showing that there is still enhancer activity in the mutants (Supplementary Fig. 8D). These findings rule out that the mutation has created a more potent SOX9 binding site that would lead to higher *Sox9* transcriptional activation as the underlying mechanism.

Pro-female factors can repress Enh13 and hence Sox9 expression

As the 3 bp deletion and 1 bp insertion do not create a more potent SOX9 BS, this prompted us to explore which other TFBS are present within Enh13, and more so, around the SOX9 BS. We hence performed JASPAR TFBS analysis on the WT Enh13 and saw the presence of putative binding sites for bipotential factors (NR5A1, WT1, GATA4) and pro-male factors (SOX9, SRY, DMRT1) as previously reported[34,36] (Fig. 4A). To our surprise, we could also identify many putative binding sites for pro-female TFs as the TCF/LEF (the WNT pathway), FOXL2, RUNX1 and WT1[32]. Moreover, overlapping to the SOX9 BS, there was a RUNX1 BS (Fig. 4B). Although typically considered a pro-ovarian factor[29], RUNX1 is expressed in both sexes at E11.5, before becoming enriched in pre-granulosa cells and downregulated in Sertoli cells[29,45,46] (Fig. 4C). Given the overlap between the RUNX1 and SOX9 binding sites, we investigated whether the mutations affected RUNX1 binding. PBM and EMSA assays confirmed RUNX1 binding to Enh13, but revealed no difference in affinity between the WT and mutant sequences (Supplementary Fig. 9A, B).

Next, to explore the effect of pro-female factors on the ability to induce *Sox9* expression via the WT Enh13, we employed Luciferase reporter assays. In the absence of any TF, Enh13 is not activated in HEK293T cells. Transfection with a combination of three critical bipotential factors: NR5A1, GATA4 and WT1 led to ~10-fold induction. The addition of FOXL2 and CHIR (agonist of the WNT pathway) did not lower enhancer activity. In contrast, addition of RUNX1 to the bipotential factors significantly lowered enhancer activity by two-fold, suggesting that the expression of RUNX1 in the ovary can repress *Sox9* expression mediated via Enh13. Combination of RUNX1, FOXL2 and CHIR together did not lower enhancer activity more than the reduction observed with RUNX1 alone (Fig. 4D). We next wanted to simulate a state where the enhancer is highly activated so that we could assess the potential repressive effect of adding pro-female factors. We hence added SOX9 to the bipotential factors and observed 133-fold enhancer induction (Fig. 4E). This time, addition of FOXL2 and CHIR significantly lowered reporter activity to 68-fold induction. Addition of RUNX1 alone also lowered enhancer activity to even lower levels (49-fold). Combined addition of pro-female factors, FOXL2, CHIR and RUNX1 presented an additive effect and further lowered reported activity to 32-fold (Fig. 4E).

Altogether, these experiments suggest that Enh13 might be normally repressed by RUNX1 and other pro-female factors and imply that the repression of *Sox9* expression, mandatory for proper ovary development, may be mediated via Enh13. It is possible that SOX9 and RUNX1 compete on partially overlapping binding sites in the testis and the ovaries, respectively.

The 3 bp deletion and 1 bp insertion mutations affect the cooperativity of TFs on Enh13 and enhance its activity

We next examined the mutation region more broadly and found it is highly conserved among mammals, both in nucleotide sequence and in the spacing between TFBS relative to the SOX9 BS (Fig. 5A). An NR5A1 binding site lies 24 bp upstream, the RUNX1 site partially overlaps with the SOX9 BS, and a GATA4 binding site is located 6 bp downstream (Fig. 5A). Notably, the RUNX1–SOX9 binding site module is fully conserved across all examined mammalian species, and the distance between this module and the adjacent NR5A1 site varies by no more than one nucleotide. The high degree of conservation in both sequence and spacing suggests that precise spatial organisation of these TFBS may be critical for cooperative binding and enhancer function, as it has been shown that even minor alterations in spacing can disrupt transcriptional synergy[49]. As SOX9 and RUNX1 binding affinities were not significantly altered (Supplementary Figs. 8, 9), we conducted a comprehensive JASPAR analysis of ~2300 vertebrate TFs, including all those expressed in the gonad at this stage. No major gain or loss of binding sites was found between WT and mutant Enh13 sequences to explain the phenotype (Supplementary Data 2; Supplementary Fig. 10A–C).

It has previously been shown that small mutations in regulatory elements could affect gene expression via alteration of the DNA helical positioning, hence modifying the 3D structure in a way that affects the cooperative binding of nearby TFBS[50,51]. To assess whether the mutations affect cooperative TF binding, we performed luciferase assays in HEK293T and COS7 cells using NR5A1, GATA4, RUNX1, and SOX9, the transcription factors with binding motifs immediately adjacent to the mutated region, conserved in both sequence and spacing, and co-expressed in the gonad prior to *Sox9* activation. Transfection of HEK293T cells with RUNX1 or any other factor alone did not induce any reporter activity (Fig. 5B, Supplementary Fig. 11 A). Co-transfection of NR5A1 and GATA4 led to a 61-fold induction of the WT Enh13, a comparable 72-fold induction for Enh13$^{SOX9*-3bp}$ (named here "−3 bp"), and a markedly stronger 107-fold activation for Enh13$^{SOX9*+1bp}$ (named here "+1 bp"). Notably, the addition of RUNX1 to NR5A1 and GATA4 reduced enhancer activity of the WT to 38-fold, but failed to repress the two mutant enhancers, which maintained elevated activity levels (70-fold for −3 bp and 77-fold for +1 bp). This suggests that the mutations impair a repressive input mediated by RUNX1 in the context of the WT enhancer. Importantly, this defect was recapitulated in COS7 cells, where the differences between the mutants and the WT were even more pronounced (Supplementary Fig. 11B). As expected, inclusion of SOX9 in the transfection cocktail strongly enhanced reporter activity, with even greater induction observed for the mutant enhancers compared to

https://doi.org/10.1038/s41467-026-71328-9

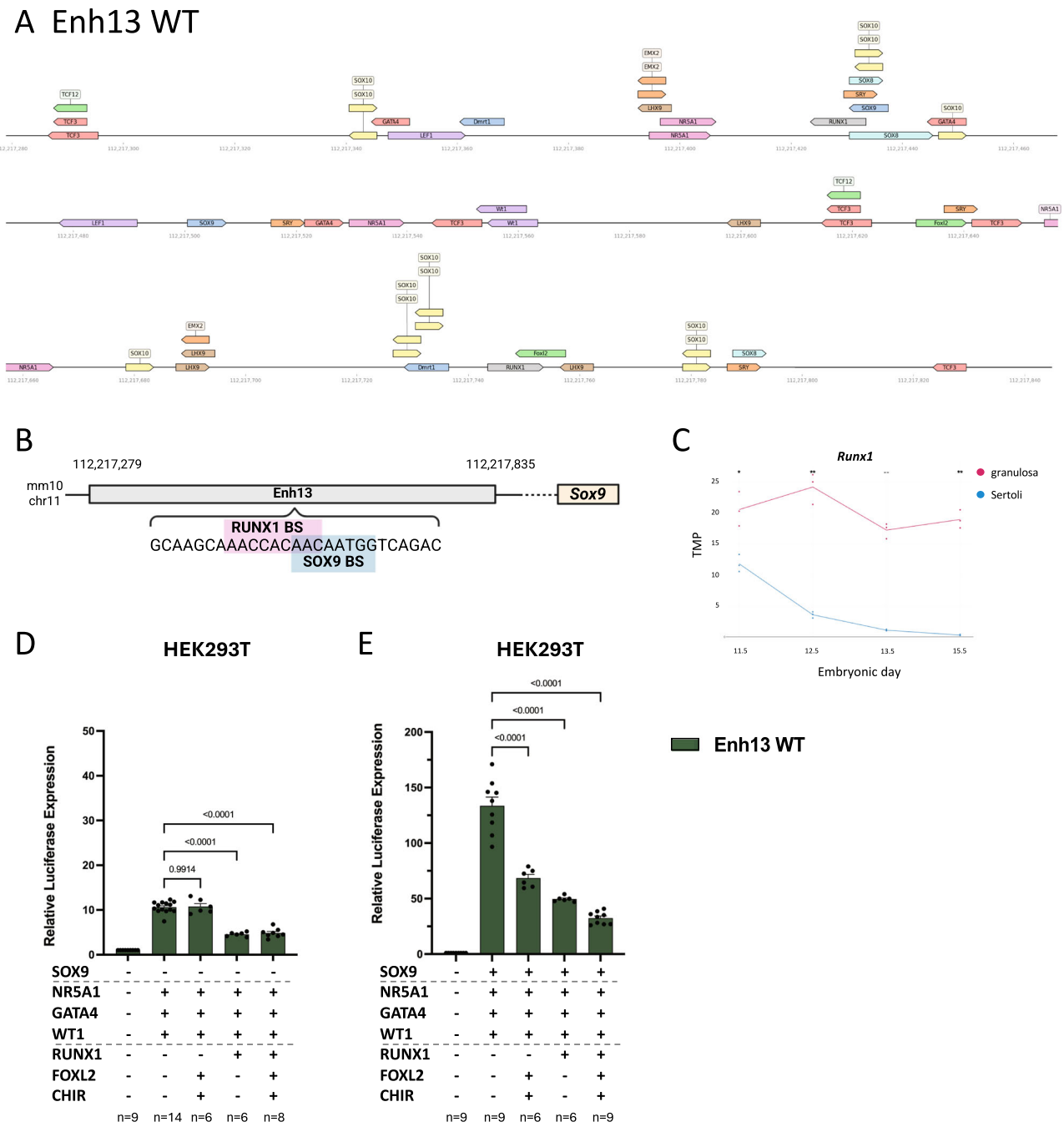

Fig. 4 | Pro-female factors can repress Enh13. A Visualization of putative binding sites analysis using the JASPAR dataset of Enh13 sequence for well-known TFs expressed in the gonad. Coloured boxes represent putative TFBS with high affinity scores. **B** Schematic representation showing the overlapping binding sites of SOX9 and RUNX1. **C** RUNX1 expression profile in sorted Sertoli and granulosa cells throughout the time window of sex determination[43]. Luciferase reporter assays performed in HEK293T cells co-transfected with luciferase reporter plasmid containing the sequences of Enh13 WT, along with bipotential factors (NR5A1, GATA4, and WT1) and with the addition of pro female factors (CHIR and FOXL2 and/or RUNX1) in the absence of SOX9 (**D**) or in the presence of SOX9 (**E**). All values were normalized to the Enh13 WT Luciferase activity in the absence of any expression plasmids. Means and SEM from at least three independent experiments are shown. Sample size for each condition is indicated on the graph, where each dot represents an independent experiment. Statistical analysis was done using a one-way ANOVA followed by Dunnett's posttest. *$P < 0.05$, **$P < 0.01$, ***$P < 0.001$, and ****$P < 0.0001$, ns- not significant. Source data are provided as a Source Data file.

the WT (120-fold for WT, 173-fold for −3 bp, and 182-fold for +1 bp) (Fig. 5B).

Together, these results indicate that the mutations render the enhancer to be less susceptible to RUNX1/NR5A1/GATA4-mediated repression, thereby facilitating *Sox9* activation. Moreover, the distinct responses of the two mutants to NR5A1 and GATA4 alone suggest that they may act through different molecular mechanisms to alter enhancer function. EMSA experiments with NR5A1 did not reveal any differences in binding between the WT and mutant probes. In contrast, EMSA with GATA4 identified a complex formed exclusively with the +1 bp probe (Fig. 5C). This result is consistent with the creation of a *de- novo* GATA binding motif (GATTG) due to the T insertion in the +1 bp mutant (Fig. 5D), a sequence known to support GATA factor binding[52]. GATA transcription factors have been reported to dimerize and enhance transcriptional output[53], raising the possibility that the new motif facilitates cooperative GATA4

https://doi.org/10.1038/s41467-026-71328-9

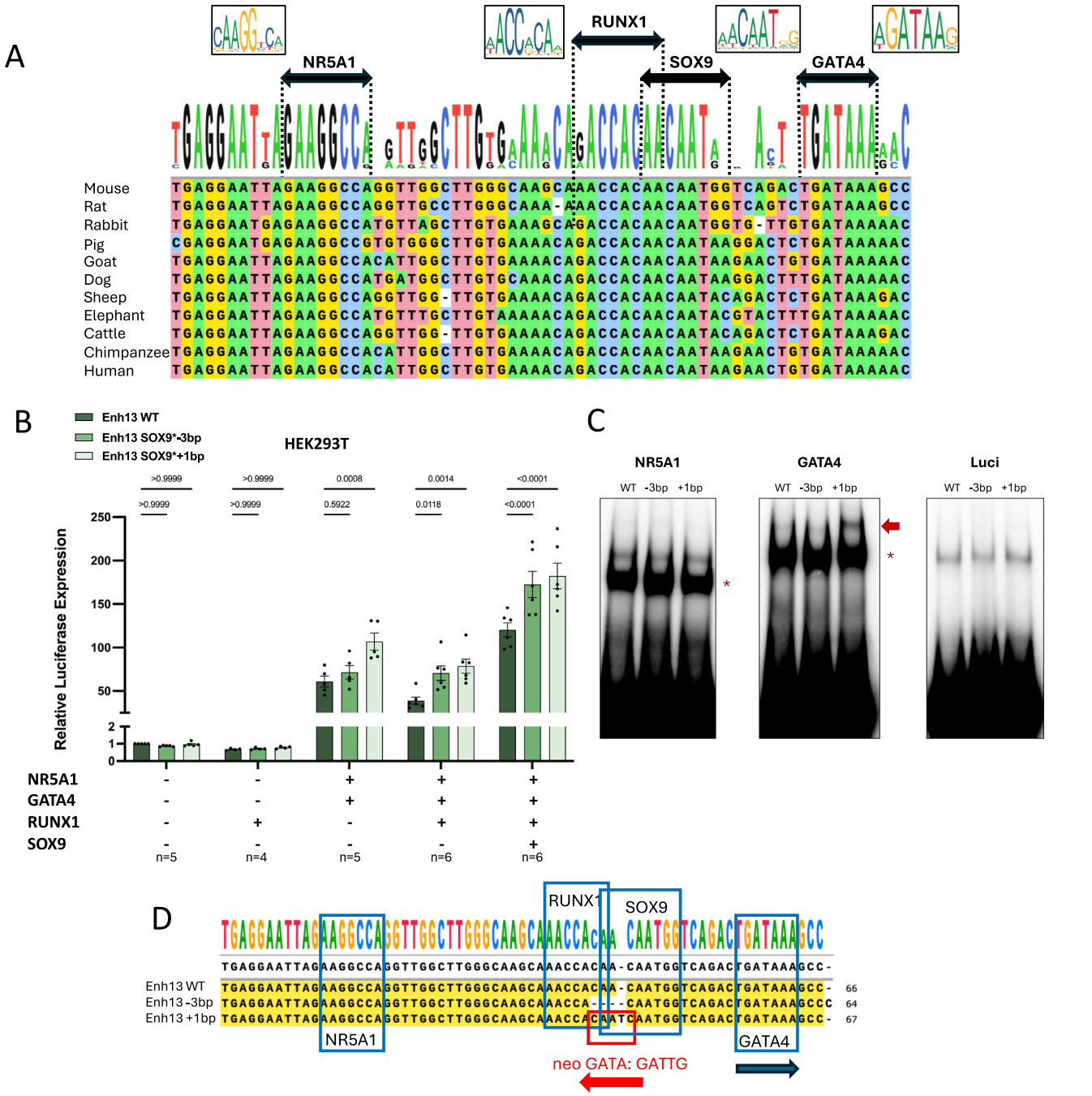

Fig. 5 | The small mutations prevent RUNX1-mediated repression, resulting in the induction of *Sox9* expression. A Enh13 sequence from 11 different mammals was compared using the Muscle tool from Snapgene. The Enh13 region around the SOX9 binding motif is presented. The locations of the NR5A1, SOX9, RUNX1 and GATA4 binding motifs are labelled (based on JASPAR). **B** Luciferase reporter assays performed in HEK293T cells, co-transfected with combinations of expression plasmids of TFs with binding sites near the SOX9 BS (RUNX1, NR5A1, GATA4, and SOX9), along with Luciferase reporter plasmid containing the sequences of Enh13 WT, Enh13$^{SOX9*-3bp}$, or Enh13$^{SOX9*+1bp}$. All values were normalized to the Enh13 WT Luciferase activity in the absence of expression plasmids. Means and SEM from at least three independent experiments are shown. Sample size for each condition is indicated on the graph, where each dot represents an independent experiment. Samples were compared to the Enh13 WT plasmid within each condition. Statistical analysis was done using a two-way ANOVA followed by Tukey's/Dunnett's posttest. *$P < 0.05$, **$P < 0.01$, ***$P < 0.001$, and ****$P < 0.0001$, ns- not significant. Source data are provided as a Source Data file. **C** EMSA using long probes containing the region presented in Fig. 5A of Enh13 WT, Enh13$^{SOX9*-3bp}$, and Enh13$^{SOX9*+1bp}$. Probes were loaded in the presence of NR5A1 (left), GATA4 (middle) or Luciferase (right) proteins. Asterisks highlight the shifted probe due to binding in the presence of NR5A1 and GATA4 protein. The arrow indicates a new GATA4 binding complex formed upon the 1 bp insertion in Enh13. This experiment was repeated independently 3 times with similar results. **D** Sequence alignment using the Muscle tool from Snapgene of Enh13 WT, Enh13$^{SOX9*-3bp}$, and Enh13$^{SOX9*+1bp}$ sequences. The consensus binding motifs of the NR5A1, SOX9, RUNX1, and GATA4 transcription factors are presented (based on JASPAR) and marked in blue boxes. The Neo GATA site found upon insertion of 1 bp (T) is marked in a red box.

binding with the adjacent native site, thereby amplifying enhancer activity.

Lastly, seeing the different response between the −3 bp and +1 bp mutants, we wanted to assess the SOX9 levels in vivo, at E11.5 gonads. To that aim, we performed whole-mount immunostaining with SF1 and SOX9 on E11.5 gonads of WT XY and XX embryos as well as embryos of Enh13$^{SOX9*+1bp-/-}$ and Enh13$^{SOX9*-3bp-/-}$ (Supplementary Fig. 12). XX WT gonads present no SOX9 expression, while XY WT gonads exhibited SOX9 expression within the SF1-positive gonadal cells. While no SOX9 protein was evident in the −3 bp mutant gonads, SOX9-positive cells were clearly present in the +1 bp mutant gonads (Supplementary Fig. 12). This is consistent with the more testicular appearance of the +1 bp mutants at E13.5 compared to the more ovotesticular phenotype of the −3 bp mutants (Fig. 2B, D).

Overall, we demonstrate that Enh13 is used for both the activation and repression of *Sox9* expression in the testis and ovary, respectively. We also show that the −3 bp/+1 bp mutations sufficiently modify the cooperative binding of TFs, to allow significantly higher activation of *Sox9* even in the absence of SRY. This surpasses the activation threshold that must not be exceeded in XX gonads, leading to SOX9 auto-activation and testis development in XX gonads.

Discussion

Mammalian sex determination hinges on a delicate balance between two opposing genetic pathways composed of pro-male and pro-female factors. While in the male pathway, there are two strong players: SRY and SOX9, where loss of either would result in XY sex reversal[5], in the female pathway, loss of an individual pro-female factor, including WT1 (-KTS)[20], FOXL2[26–28], RUNX1[29] and components of the WNT pathway[21–25] do not lead to XX sex reversal in mice. It is only when two pro-female factors or more are deleted together, that the XX male phenotype starts to appear at embryonic stages[29–32]. Therefore, it is striking that a single nucleotide insertion within a non-coding regulatory element, located more than 500 kb upstream of the *Sox9* gene, can lead to a robust XX female-to-male phenotype, not generated by ablation of any known pro-female gene.

Enh13 was previously considered a strictly testis-specific enhancer, as its deletion[34,35] as well as mutations in the SOX9 and SRY binding sites we previously described, and in a downstream GATA4 site[36,54,55], all lead to XY male-to-female sex reversal. No ovarian phenotype related to Enh13 was observed. Two hypotheses can be raised regarding the function of Enh13 in ovary development: either Enh13 plays an active repressive role in the ovarian environment, or its WT nucleotide sequence makes it refractory to activation in the absence of SOX9 or SRY. Our reporter assay experiments suggest that RUNX1, and later on, additional pro-female factors, are able to repress the enhancer, mediating *Sox9* repression in the ovary that is mandatory for proper ovary development. The two mutations presented here show that subtle alterations in the Enh13 sequence can overcome this repressive state, allowing low-level activation of *Sox9* independently of the SRY protein. This minimal activation would be enough to trigger the self-amplification loop. By surpassing the threshold level of SOX9 protein in XX supporting cell precursors, the system initiates and sustains itself. Interestingly, three 46, XX male patients were described who carry a small duplication containing the human orthologue of Enh13[37,38]. Although the mechanism was never experimentally resolved, this may reflect either a structural effect of enhancer duplication or a titration of inhibitory factors, both of which could relieve repression and permit *SOX9* activation in the absence of *SRY*. Indeed, it has previously been shown that overexpression of *Sox9* in XX mice or human gonads can alone induce testis development in the absence of *Sry*[16,17]. Pigs also present XX male sex reversal (SRY-negative), and the causative region was mapped to the *SOX9* locus. As sequencing of the *SOX9* gene, promoter, or the TESCO enhancer did not reveal the variant[56] it suggests that variants in the Enh13 pig homologue may be involved in this phenotype.

Our data demonstrate that subtle sequence changes within the SOX9/RUNX1 binding site of Enh13 do not enhance SOX9 or RUNX1 binding directly but instead disrupt local repressive inputs and modulate the cooperative function of neighbouring transcription factors. Moreover, the hypothesis of a role for SOX9 at E11.5 in XX gonads is unlikely, given that SOX9 is cytoplasmic prior to sex determination in both XX and XY gonads[40,47] and is actively excluded from the nucleus through an exportin-dependent nuclear export mechanism[57].

The acquisition of activating capacity by the Enh13 mutants in the absence of SRY or SOX9 may instead be linked to the fact that, in both mutants, the RUNX1 and GATA4 binding sites are brought closer together, which could promote physical interactions between the transcription factors occupying these DNA motifs. Indeed, it has been shown in megakaryocytes that RUNX1 can interact with GATA1 through the zinc-finger domains of GATA1[58], which are highly conserved with those of GATA4. In these cells, both transcription factors can bind in close proximity on enhancers to activate gene expression[58]. This mechanism is evolutionarily conserved up to *Drosophila*, where the orthologous proteins Srp and Lz (the fly counterparts of GATA and RUNX, respectively) interact to control the expression of genes in fly blood cells[59]. In our case, for the −3 bp mutant, the deletion brings RUNX1 and GATA4 closer together on chromatin (Fig. 6, XX − 3 bp). At the chromatin level, a 3 bp deletion shifts the two DNA motifs by roughly one third of a helical turn, which can be sufficient to place them face-to-face rather than back-to-back (or vice versa), thereby strongly affecting the likelihood of protein–protein interactions on chromatin. Depending on the helical phasing of the DNA, this configuration may allow a functional interaction between RUNX1 and GATA4, resulting in transcriptional activation. This interpretation is supported by the remarkable evolutionary conservation of the spacing between the RUNX1 and GATA4 binding sites, which varies by no more than a single nucleotide across all examined mammalian species (Fig. 5A). It may normally serve to prevent physical contact between RUNX1 and GATA4.

In the +1 bp mutant, the effect is even stronger, but similar, since a neo-GATA motif is created adjacent to the RUNX1 binding site (Fig. 6, XX + 1 bp). Consequently, the initial activation is likely driven by an extra-physiological interaction between RUNX and GATA factors. Our results align well with the stronger testis phenotype observed in the +1 bp mutants, compared to the more partial sex reversal and ovotestis phenotype seen in the −3 bp mutants (Fig. 2B, D). Indeed, at E11.5 gonads, SOX9 expression can already be seen in the +1 bp mutants, but not yet in the −3 bp gonads (Supplementary Fig. 12).

We hence propose the following model (Fig. 6): In XY gonads, SRY, particularly through its functional interaction with NR5A1[7], activates Enh13 and induces *Sox9* expression, which subsequently reinforces its own expression through auto-activation, leading to testis development (Fig. 6, XY WT). In XX gonads, bipotential factors, including RUNX1, bind Enh13 and mediate repression of *Sox9*. Around E12.0, upon the onset of FOXL2 expression, pro-female factors act cooperatively to fully repress *Sox*9, thereby allowing ovary development (Fig. 6 XX WT). In the −3 bp mutant, the mutation alters the conformation of Enh13 by bringing RUNX1 and GATA4 proteins closer together on chromatin. Under these conditions, NR5A1-, RUNX1- and GATA4-containing complexes acquire sufficient activating capacity to weakly induce *Sox9* expression, reaching the threshold required for its auto-activation, at which point SOX9 replaces RUNX1 on Enh13. This initiates ovotestis development, which is subsequently resolved into a testis (Fig. 6, XX−3 bp). In the +1 bp mutant, the mutation creates an additional GATA4 binding site in close proximity to RUNX1. This results in higher levels of SOX9 protein, which more efficiently reinforces *Sox9* autoregulation, leading to a milder ovotestis phenotype that more closely resembles a testis and ultimately resolves into a testis

https://doi.org/10.1038/s41467-026-71328-9

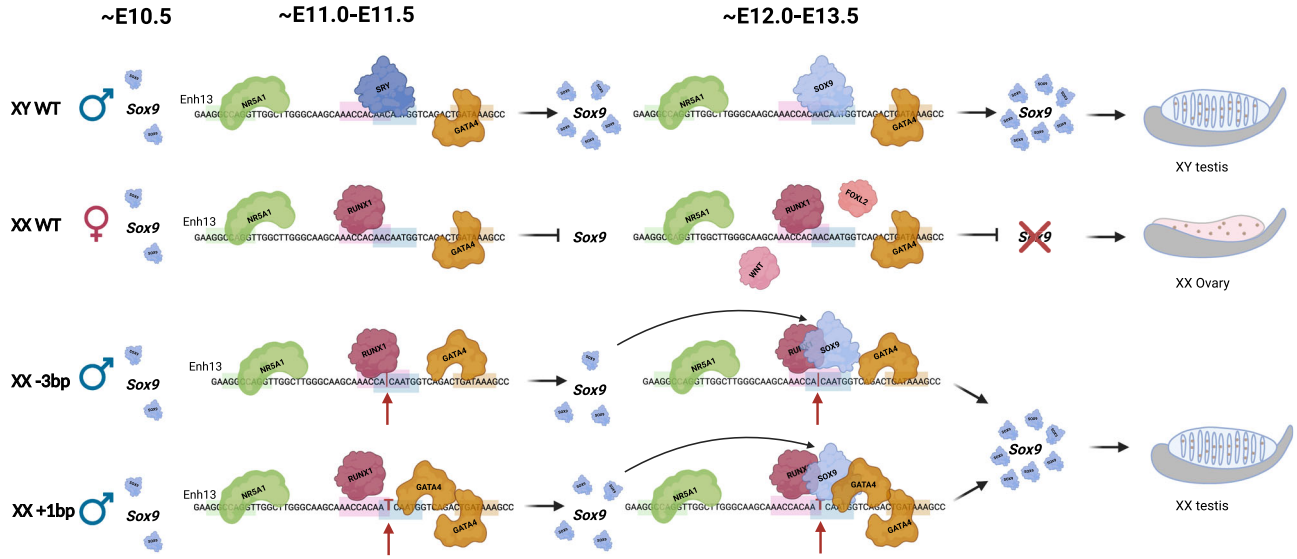

Fig. 6 | Proposed mechanism of Enh13 activity in XY WT, XX WT, and mutant gonads. Schematic proposed model of cooperative binding of NR5A1, SRY/SOX9, and GATA4 in XY males or NR5A1, RUNX1, and GATA4 and other pro-female factors in XX females, and their effect on *Sox9* expression in XY WT and XX WT gonads. The two XX Enh13 $^{SOX9^{*}-3bp}$, XX Enh13 $^{SOX9^{*}+1bp}$ mutant sequences are presented along with a model describing the proposed mechanism leading to *Sox9* activation. Upon the mutations, *Sox9* is activated, later further upregulating itself. WT- *Wild Type*. "Created in BioRender. Gonen, N. (2026) https://BioRender.com/ltb9lqy".

(Fig. 6, XX + 1 bp). Taken together, both mutations share a common feature: they bring RUNX1 and GATA4 proteins closer together on chromatin, either directly, in the −3 bp mutant, by shortening the distance between their binding motifs, or indirectly, by creating a de novo motif that allows GATA4 to bind in very close proximity to RUNX1 on chromatin.

Alterations in TFBS affinity have been shown to cause severe developmental phenotypes[60]. Notably, single-nucleotide variants within the ZRS enhancer of the *Sonic Hedgehog* (*Shh*) gene were found in human patients with polydactyly[61]. These variants, which affect intrinsically low-affinity ETS binding sites, were shown to increase ETS factor binding, leading to ectopic *Shh* expression and limb malformations[61]. In contrast, our data indicate that the gain-of-function observed at Enh13 does not arise from increased transcription factor binding affinity. Instead, it results from a structural alteration of the enhancer itself, likely inducing a three-dimensional reorganization of bipotential and ovarian transcription factors along the Enh13 DNA. This reconfiguration alters their cooperative interactions on chromatin, thereby altering the transcriptional output of the enhancer. This change grants them a slight activating capacity, sufficient to activate *Sox9* in the ovary. Indeed, it has been shown and proposed that the distance between nearby TFBS and the surrounding sequence can dramatically affect the cooperative binding of TFs, eventually altering gene expression[50,51,62]. Our phenotype and mechanism highlight Enh13 as an exceptional in vivo model for studying these aspects: the mutations are not lethal as in other cases, and their outcome is easy to characterize, i.e., altering the sex of the organism.

Finally, our study raises the question of how Enh13 becomes activated in the mutant context at the level of chromatin accessibility. Our previous ATAC-seq analyses[43] revealed that Enh13 opens specifically in XY gonads at E11.5, while remaining closed in XX gonads, suggesting that enhancer opening in males may depend on SRY. Consistent with this idea, several members of the SOX family, including SOX2, SOX11[63], and SOX9[64], have been described as pioneer transcription factors. In the present study, however, the ectopic activation of *Sox9* observed in both mutant contexts reasonably suggests that Enh13 becomes accessible in XX mutant gonads, suggesting that enhancer opening can occur independently of SRY. This observation raises the critical question of which transcription factor(s) may act as pioneer factor(s) to initiate Enh13 activation in this context. GATA, RUNX and NR5A2 proteins have been shown to act as pioneer factors[65–67]. We therefore speculate that changes in Enh13 organization in our mutants may activate the pioneering capacity of RUNX and GATA factors, thereby contributing to the opening of Enh13. Addressing this issue will require future analyses of the temporal dynamics of Enh13 chromatin opening in XX mutant gonads, particularly around E11.5.

In conclusion, we hypothesize that upon the entire deletion of Enh13[34,35] or mutations in the SOX9/SRY/GATA4 TFBS[36,54,55], *Sox9* expression could not be activated, leading to XY female development, yet no XX male development could be seen, as testes could not develop without *Sox9* activation. It seems that the +1 bp / −3 bp mutations allow decoupling *Sox9* repression from *Sox9* activation, enabling us to decipher a critical role of Enh13 during ovary development. These findings indicate that *Sox9* is both activated and repressed using the same regulatory element, and it depends on the factors binding to Enh13 that will eventually determine if *Sox9* gets activated or repressed. These findings pave the way for structural analyses of DNA-protein interactions at Enh13, aiming to understand how minor sequence changes translate into three-dimensional differences in enhancer conformation and regulatory output between the WT and the two mutants. This study not only uncovers a sexually dimorphic function of Enh13 but also highlights the broader principle that enhancer activity can be profoundly influenced by subtle structural variations in sequence architecture. These findings open new perspectives for investigating other developmental enhancers whose function may similarly depend on precise spatial organisation and cooperative transcription factor interactions, laying the groundwork for a structural, sequence-level understanding of enhancer grammar in diverse developmental contexts.

Methods

Animal Ethics Statement

All animals were maintained with appropriate husbandry according to Bar Ilan University ethics protocols 11-02-2020, 1-11-2020, and 2306-117-11. All mice were maintained under specific pathogen-free conditions. Animals were housed at a temperature of 20–24 °C with a

relative humidity of 35-65% under 12 hour light-12 hour dark cycle. All mice strains generated were maintained on a C57BL/6 J genetic background. Primers used for genotyping are listed in Table S1. At least ten different animals of each genotype from all mouse strains were analysed.

Design and preparation of sgRNAs mRNA

Guide RNAs targeting each transcription factor binding site (TFBS) were designed using the IDT CRISPR/Cas9 design platform (https://eu.idtdna.com). Candidate guides were selected based on their position relative to the center of the TFBS, considering that Cas9 cleavage typically occurs approximately 3–4 bp upstream of the PAM sequence. To prepare the crRNA–tracrRNA duplexes, crRNAs for all guides (sgRNA sequences are provided in Table S2) and tracrRNA (IDT, 224893246) were each resuspended to a concentration of 200 μM in Nuclease-Free Duplex Buffer (IDT, 11-01-03-01). Equal volumes of crRNA and tracrRNA were then combined at a 1:1 ratio to generate a final duplex concentration of 100 μM. Duplex formation was achieved by heating the mixture at 95 °C for 5 min, followed by gradual cooling to room temperature. The annealed complexes were stored at −20 °C for up to two weeks until use.

CRISPR/Cas9 ribonucleoprotein (RNP) complexes were assembled immediately before electroporation. The RNP mixture was prepared in Opti-MEM (Thermo Fisher Scientific, 31985-062) and consisted of 1.2 μM Cas9 Nuclease V3 (IDT, 1081059) and 6 μM sgRNA. In experiments where two RNP complexes were introduced simultaneously, the concentration of each sgRNA was adjusted to 3 μM. The assembled RNP mixture was incubated for 10 minutes at room temperature and subsequently kept on ice until electroporation of zygotes.

Zygote harvesting and electroporation

For zygote collection, C57BL/6J female mice aged 4–7 weeks were hormonally stimulated by intraperitoneal injection of 5 IU PMSG (Pregnant Mare Serum Gonadotropin; ProSpec, hor-272). After 48–50 hours, females received a second intraperitoneal injection of 5 IU hCG (Human chorionic gonadotropin; Sigma Aldrich, CG10). Immediately following hCG administration, females were paired with adult C57BL/6 J males at a 1:1 ratio. The following morning, females were examined for the presence of a vaginal plug (VP). Females with a confirmed VP were euthanized by cervical dislocation, and their oviducts were dissected to isolate fertilized zygotes.

The oviducts were removed and the ampulla was gently opened to release cumulus–oocyte complexes into M2 medium (Sigma Aldrich, M7167) supplemented with 300 μg/ml hyaluronidase (Sigma Aldrich, H4272) to disperse the surrounding cumulus cells. Zygotes were collected using a mouth-controlled glass pipette and transferred into a dish containing 2 ml of fresh M2 medium. They were subsequently washed through several M2 droplets to ensure complete removal of residual cumulus cells. Cleaned zygotes were then transferred to KSOM culture medium (Mercury, MR-106-D) and incubated for 30 minutes in a flat-bed CO_2 incubator (5.3% CO_2, 5% O_2 at 37 °C; Esco, Miri 2070047). Embryos exhibiting visible polar bodies and pronuclei were selected, rinsed in M2 droplets, followed by three washes in Opti-MEM, and finally transferred into the electroporation chamber containing the prepared RNP mixture.

Electroporation was carried out using a NEPA21 electroporator (NepaGene). A series of pulses was applied to transiently disrupt the zona pellucida and facilitate entry of the CRISPR/Cas9 ribonucleoprotein complexes into the zygotes. Depending on the experimental setup, either a large glass electrode plate (CUY505P5, 5 mm gap) containing 50 μl of RNP solution and 20–150 embryos or a small glass electrode plate (CUY501P1, 1 mm gap) containing 5 μl of RNP solution and 5–50 embryos was used.

For the large electrode plate, poring pulse parameters were set to 225 V, 1 ms pulse width, 50 ms interval, and 4 pulses. Transfer pulses were applied at 20 V with a 50 ms pulse width, 50 ms interval, and 5 pulses. For the small electrode plate, poring pulses were delivered at 40 V with a pulse width of 3.5 ms, a 50 ms interval, and 4 pulses. Transfer pulses were set to 5 V with a 50 ms pulse width, 50 ms interval, and 5 pulses. Electrical impedance was measured both before and after embryo loading according to the manufacturer's instructions.

Following electroporation, embryos were washed sequentially in M2 and KSOM droplets and then cultured overnight in KSOM medium in a CO_2 incubator (5.3% CO_2, 5% O_2 at 37 °C). Embryos that progressed to the 2-cell stage were subsequently transferred surgically into the oviducts of pseudopregnant CD1 recipient females.

gDNA isolation and genotyping genetically altered mice

Genomic DNA (gDNA) was extracted from tail biopsies of embryos or ear punch samples from adult mice. For adult tissue, ear punches were incubated for 15 min at 95 °C in lysis buffer containing 10 mM NaOH and 0.1 mM EDTA (pH 8), followed by neutralization with 40 mM Tris-HCl (pH 5). Embryonic samples were processed using the PCRBIO Rapid Extract Lysis Kit (PCRBIO, PB15.11-S) according to the manufacturer's instructions.

Founder mice carrying mutations in the SOX9 or combined SOX9 and SRY binding sites within Enh13 were initially screened by Sanger sequencing of a 616 bp PCR fragment spanning the entire Enh13 region (genotyping primers listed in Table S1). Identified founders were crossed with C57BL/6 J mice to establish germline transmission. F1 offspring were verified by Sanger sequencing, after which mutation-specific PCR assays were designed for routine genotyping. Heterozygous F1 animals were crossed to establish stable mutant lines. PCR products were purified using either the Universal DNA Purification Kit (TIANGENE, TI-DP214-03) or the EPPiC Fast Kit (A&A Biotechnologies, 1021-500 F) before sequencing. INDEL mutations in founders and F1 pups were analyzed using the online tool DECODR. For samples carrying sequential mutations within the same allele, TA cloning (Promega pGEM®-T, A3600) was performed to resolve the mutation structure. The purified 616 bp Enh13 PCR fragment was ligated into the pGEM®-T vector, transformed into competent E. coli (NEB, C3019), plated on LB agar containing 100 μg/mL ampicillin, and incubated overnight at 37 °C. Individual colonies were isolated, plasmid DNA was purified using the NucleoSpin Plasmid EasyPure Kit (Macherey-Nagel, 740727), and inserts were sequenced and analyzed using BLAST.

For routine genotyping, the 616 bp Enh13 fragment was amplified and digested with BstXI FD (Thermo Scientific, FD1024). This enzyme cleaves the wild-type allele into fragments of 367 bp and 249 bp but does not cut alleles carrying mutations in the SOX9 binding site, which remain as a 616 bp fragment. Digested products were run on a 2% agarose gel.

All PCR reactions were performed using 2X Red PCR Master Mix (PCRBIO, PB10.23-10) according to the manufacturer's instructions. Chromosomal sex of all mice and embryos was determined by PCR (primers listed in Table S1).

Time mating, gonad harvesting, preparation and imaging

Gonads were harvested from embryos and mice carrying the desired mutations. Embryos were collected following timed matings at embryonic day E12.5 or E13.5, with day 0.5 defined by the detection of a vaginal plug (VP). Bright-field images of gonads were acquired using a Nikon Eclipse Ts2R microscope with an exposure time of 10 ms and processed using NIS-Elements D software.

For immunostaining of the gonads from E13.5 embryos and 6-week-old mice were dissected and fixed overnight at 4 °C in 4% paraformaldehyde (Sigma Aldrich, P6148) prepared in phosphate-buffered saline (PBS). Samples were then washed three times in PBST (PBS containing 0.1% Triton; Sigma Aldrich, 9002-93-1) at room

temperature, incubated overnight in 20% sucrose (Fisher BioReagents, BP220-1) at 4 °C, embedded in OCT compound (Leica, 14020108926), and stored at −80 °C until immunostaining.

Immunofluorescence staining

Immunofluorescence staining for E13.5, E15.5, P1, and 6-week samples was performed on 10µm-thick sagittal cryostat sections (Leica, CM3050-S). Antigen retrieval was performed for embryonic samples with DAKO (Target retrieval solution, Agilent, S1699) at 65 °C for 30 min. Samples were then blocked in PBST containing 10% donkey serum (Sigma Aldrich, D9663) for 1 hour at room temperature (RT) and incubated with primary antibodies (diluted in PBST containing 1% donkey serum) overnight at 4 °C. Following three PBST washes, secondary antibodies were added for 1 hour at RT. Slides were then washed, dried, and mounted (Polysciences 18606-20). All immunofluorescence slides were also stained with 4′,6-diamidino-2-phenylindole (DAPI; Invitrogen, D1306) to visualize nuclear DNA.

For E11.5 gonads, whole-mount immunostaining was performed. Gonads were fixed in 4% paraformaldehyde for 20 minutes at RT. Blocking was performed in 10% donkey serum in 0.3% PBST for 3 hours at RT. Samples were then incubated with primary antibodies in a solution of 10% donkey serum in 0.3% PBST at 4 °C overnight. After six washes with PBST, samples were incubated overnight with secondary antibodies and DAPI in a solution of 10% donkey serum in 0.3% PBST at 4 °C. The next day, samples were washed and transferred onto a glass slide with mounting media (Polysciences 18606-20).

All primary and secondary antibodies, as well as dyes used are listed in Table S3. Images were obtained with a Leica Microsystems SP8 confocal microscope.

RNA isolation, cDNA preparation, and Quantitative Real-Time Polymerase Chain Reaction (qRT-PCR)

RNA was isolated from a pair of E13.5 embryos by dissecting out the gonad-mesonephros complexes. The gonad was separated from the mesonephros, and a pair of gonads was snap frozen and stored in −80 °C until isolation. For 6-week-old gonads, RNA was isolated using Qiagen RNeasy Plus mini kit (Qiagen, 74134) and from E13.5 gonad pairs using Qiagen RNeasy Plus micro kit (Qiagen, 74034). RNA concentration was measured using a NanoDrop spectrophotometer. cDNA synthesis was performed using SuperScript™ III Reverse Transcriptase (Thermo Scientific, 18080085) with 1 µg of RNA from adult gonads or 200 ng from E13.5 gonads, following the manufacturer's instructions.

qRT-PCR reactions were performed in duplicate using PowerSYBR Green PCR Master Mix (Thermo Scientific, AB-4367659) with 140 nM forward and reverse primers (Table S4), and run on a QuantStudio 1 Real-Time PCR System (Thermo Scientific). Gene expression was analysed using the comparative CT (ΔΔCT) method and normalized to the housekeeping gene Hprt. Statistical analysis was performed using GraphPad Prism 9. Data were analysed by one-way ANOVA followed by Dunnett's post-hoc test, with $p < 0.05$ considered statistically significant. Dataset normality was evaluated using the Shapiro–Wilk test, and potential outliers were assessed using Grubbs' test. The number of gonads analysed for each stage is indicated in the corresponding graphs.

RNA-seq and library prep

Gonad pairs of E12.5 mice were dissected, separated from the mesonephros and snap-frozen in liquid nitrogen. RNA was extracted using Qiagen RNeasy Plus micro kit (Qiagen, 74034). 140 ng of total RNA was taken from each sample for library preparation. mRNA was transcribed to cDNA and prepared into libraries using Poly(A) mRNA Magnetic Isolation Module (NEB, E7490S), along with NEBNext UltraExpress RNA library prep kit (NEB, E3330S) and cleaned using AMPure beads (Beckman Coulter, Bc-a63881) according to manufacturer's instructions. Unique indexes were added to each sample using ++NEBNext Multiplex Oligos for Illumina kit (NEB-E6440S) according to the manufacturer's instructions and cleaned using AMPure beads. cDNA and library concentrations were analysed using Qubit ds HS Assay Kit (Invitrogen, 2326054) and sample size distribution using Tapestation with high sensitivity D1000 tape (Agilent, 5067-5585). Samples were pooled together to create a 2 nM library and sequenced with 50 bp paired-end (PE) reads on the Next-Seq NovaSeq X Plus 1.5B at the *Nancy and Stephen Grand Israel National Center for Personalized Medicine* (G-INCPM) facility at Weizmann Institute with ~70 million reads per sample.

RNA-seq mapping and differential expression analysis

FastQ files were processed using the nf-core/rnaseq pipeline v3.12.0. Briefly, read quality controls were performed with FastQC. Sequencing adapters were removed with TrimGalore!. Reads were mapped on the mm10/GRCm38 reference genome from Gencode (M25) with STAR. Gene quantification as read counts and TPM (Transcript Per Million) was obtained using RSEM. Read count matrix was filtered to exclude lowly expressed genes (genes with less than 10 reads and/or TPM value less than 10). Non-protein-coding genes were filtered out in the subsequent analysis. Sample correlation (Spearman) and PCA were performed with R (corr and prcomp functions) using the filtered read counts normalized by library size (sizeFactor) with DESeq2. After inspection of the correlation and the PCA, we excluded the XY WT replicate 3 because it was too different from the other two replicates. The embryo of this sample had 2 more tail somites than the two other replicates.

Differential expression analysis was performed on the filtered read count matrix using DESeq2 using "LRT" (Likelihood Ratio Test). Genes with log2(FoldChange) < −0.5 and log2(FoldChange) > 0.5, as well as an adjusted p-value < 0.01 were considered as differentially expressed.

Gene expression values (filtered read count matrix normalized by library size) of the differentially expressed genes were transformed as z-scores, clustered into groups according to their expression profiles using hclust and "ward.D2" method, and represented as a heatmap using ComplexeHeatmap. The optimal number of clusters was assessed using the best.cutree function from the Jlutils R package (https://github.com/larmarange/Jlutils), with a minimum of four possible clusters. Samples were ordered according to the hierarchical clustering ("ward.D2") and split into three groups.

Cloning of Luciferase vectors

The following expression plasmids for luciferase assays were used: pCMV3-hWT1-KTS-C-HA (SINO BIOLOGICAL, Ref: HG12282-CY), pCS2-Flag-FOXL2 (Addgene, Ref 153135), pcDNA3-Flag-hSOX9 (A gift from Gerd Scherer to FP, described in ref. 68, pcDNA3.1-Flag-Runx1-FL (Addgene, Ref: 14585), pCS2-HA-GATA4 (A gift from Segei Tevosian to FP) pcDNA3-2X-MYC-hNR5A1(a gift from FP as described in ref. 36. Empty pcDNA3 vector was used as a control.

For stimulation of the Wnt pathway, 6uM CHIR-99021 (Cell signaling, 54290) was added to the media 1 hour before transfection. To confirm stimulation of the Wnt pathway, a commercial TOP/FOP-Flash reporter assay was performed. 2.5 × 104 HEK cells were plated on 96-well white chimney cell plates (Greiner, 655098) 24 hr prior to transfection. Cells were transfected with either TOPFlash or FOPFlash reporter plasmids along with pTK-RL plasmid (Promega) with regular media or with media in the presence of 6 µM CHIR. After 24 h, cells were analyzed using the Dual-Glo® Luciferase Assay System (Promega, E2980). Luciferase intensity was normalized to the Renilla to normalize transfection efficiency. Cells transfected with the TOP plasmid, in the presence of 6 µM CHIR, showed 43-fold induction compared to cells transfected without the addition of CHIR, while FOP-transfected cells showed no change upon the addition of CHIR, confirming the ability of 6 µM CHIR to activate the Wnt pathway.

To clone DNA inserts into luciferase plasmids, gDNA was extracted from earpieces of XY Enh13 WT, XX Enh13$^{SOX9*-3bp\ -/-}$ and XX Enh13$^{SOX9*+1bp\ -/-}$ homozygous mice using DNeasy Blood & Tissue kit (Qiagen, 69504). Enh13 was amplified along with the addition of restriction enzymes BglII and HindIII sites using 2X Phusion (NEB, M0531L, Primers used in Table S1). DNA inserts were digested using BglII and HindIII enzymes (Thermo, K1991) and ligated into the pGL4.26 plasmid (Promega) between the BglII and HindIII sites in the multiple cloning site using a DNA ligation kit (Takara, 6022). Sanger sequencing was used to validate each ligation product.

Luciferase assay

Luciferase assays were performed in HEK293T (human cells) or COS7 cells (monkey cells). 2.5 × 104 cells were plated on 96-well white chimney cell plates (Greiner, 655098) 24 hours prior to transfection. Cells were transfected with either empty or Enh13 WT/ Enh13$^{SOX9*-3bp}$/ Enh13$^{SOX9*+1bp}$ pGL4.26 plasmids (100 ng) and expression plasmids for transcription factors, along with Renilla Luciferase pLR-TK vector (Promega) 1 ng for HEK293 cells and 15 ng for COS7 cells. In Fig. 4D, E, Supplementary Fig 8D. 20 ng of each TF was used and topped up with empty pcDNA3 plasmid to 120 ng total. In Fig. 5B and Supplementary Fig. 11A-B, TFs were added in a way that mimics the ratio of TF present at E12.5 granulosa cells according to TPM values from RNA-Seq of E12.5 granulosa cells[45]. TPM values of E12.5 granulosa cells are as follows: GATA4-385.7, NR5A1-173.6, RUNX1-24.2, SOX9-39.0. Therefore, the following amount was added from each TF: GATA4-61.96 ng, NR5A1-27.88 ng, RUNX1-3.89 ng, SOX9-6.27 ng and topped up to 100 ng total for conditions not including all factors. Transfection was performed using PolyJet transfection reagent (SignaGen, SL100688) at a 3:1 polyJet: DNA ratio. Luciferase activity was measured 24 hours following transfection using the Dual-Glo® Luciferase Assay System according to the manufacturer's instructions (Promega, E2980).

To calculate relative Luciferase activity, Firefly Luciferase values were normalized to the Renilla Luciferase values and then to the average of the empty pcDNA3 vector. For Luciferase assays in COS7 cells, we normalized the Firefly luciferase values to that of the average of the empty pcDNA3 vector without normalizing first to Renilla, as GATA4, among other TFs, is known to dramatically affect Renilla activity in COS7 cells[69]. All experiments were performed in duplicate of technical repeats and were repeated at least three independent times or more. Statistical analyses were carried out using the Prism 9 software (GraphPad). Two-way ANOVA was performed to compare the samples, followed by Tukey's/Dunnett's. In Luciferase assays comparing only the Enh13 WT plasmid, one-way ANOVA was performed followed by Dunnett's post-test.

Protein Binding Microarray (PBM) and analysis

Transcription factor (TF) binding characterization was performed using protein binding microarrays (PBMs), as described in refs. 70,71. Briefly, commercial microarrays (Agilent Technologies) containing all possible 10-mer or 9-mer sequences were converted to double-stranded DNA via solid-phase primer extension using Thermo Sequenase DNA Polymerase (Cytiva, Catalogue #: E79000Y) and a deoxynucleotide triphosphate (dNTP) mixture (dATP, dCTP, dGTP, dTTP).

Microarrays were then blocked with 2% (wt/vol) non-fat dry milk (Sigma, Catalog #: M7409) and incubated with the TF of interest (pcDNA3-Flag-hSOX9; pcDNA3.1-Flag-Runx1-FL), expressed using the TnT® Quick Coupled Transcription/Translation System (Promega, Catalog #: L1170, L2081). Binding reactions were carried out in different buffers depending on the protein. RUNX1 was incubated in a PBS-based buffer, with 1% (wt/vol) non-fat dry milk, 51.3 ng/µl salmon testes DNA (Sigma, Catalog #: 16-201), 0.2 µg/µl bovine serum albumin (BSA) (NEB, Catalog #: B9200), and 1 mM dithiothreitol (DTT). SOX9 buffer contained 10 mM Tris-HCl (pH 7.5), 10 mM NaCl, 1 mM $MgCl_2$, 0.01 mM $ZnCl_2$, 1% glycerol, 1% (wt/vol) non-fat dry milk, 10.4 ng/µl Poly(dI-dC) (Sigma, Catalog #: P4929), 0.2 µg/µl bovine serum albumin (BSA) (NEB, Catalog #: B9200), and 1 mM dithiothreitol (DTT).

Pre-incubated protein binding mixtures were applied to individual microarray chambers and incubated for 1 h at room temperature. Microarrays were then subjected to two sequential washing steps: first with PBS/0.5% (vol/vol) Tween-20 for 3 min, followed by PBS/0.01% Triton X-100 for 2 min. After protein incubation and washing, microarrays were incubated for 1 h at room temperature with fluorescently labelled antibody diluted in protein binding buffer supplemented with 2% milk, according to the epitope tag of the protein. The antibody used was Alexa488-conjugated DYKDDDDK antibody (FLAG) (Cell Signaling Technology, Catalog #: 15008S; dilution 1:40). Following antibody incubation, microarrays were washed with PBS / 0.05% (vol/vol) Tween-20 for 5 min twice, followed by PBS for 2 min. All washing steps were performed in Coplin jars at room temperature with shaking at 125 rpm.

Fluorescence signals of the bound proteins were recorded at 488 nm using a GenePix® 4400 A scanner at 2.5 µm resolution. Signal intensities were extracted using GenePix Pro 7.0 software, and the median pixel intensity was reported for each DNA probe. To identify DNA motifs recognized by the TF of interest, we analyzed all possible 8-base sequences (8-mers) or 7-base sequences (7-mers) as previously described[70]. In brief, DNA features were grouped into two sets − those containing the 8-mer/7-mer (foreground) and those without (background). We then compare the top half of signal intensities from both sets using a modified Wilcoxon-Mann-Whitney statistic, which helps identify the most enriched 8-mer/7-mer, termed the "seed" of the motif. Next, we assess the contribution of each nucleotide position within this seed by evaluating all possible nucleotide variants at each position, and the motif was further refined by including gaps at positions with high variability. Finally, we convert the derived motif into a position weight matrix (PWM), allowing for a quantitative representation of the TF's binding specificity. PBM binding affinity visualization along the WT and mutant Enh13 sequence was performed by looking at the E-score, the Z-score and the fluorescent intensity for SOX9 and RUNX1 transcription factors on each 8-mers composing the Enh13 sequence. Plots were generated in R, using ggplot2.

JASPAR Analysis

We extracted Position Probability Matrices (PPMs) for 16 transcription factors (TFs) from the JASPAR 2024 database, selecting a combination of murine and human matrices due to the high conservation of TF binding sites between species. As JASPAR often provides multiple matrices per TF, we manually selected one or two per factor that best represented the core binding motif, minimizing noise in the analyses.

To compare the binding potential of Enh13 in its wild-type (WT) and its mutant forms (1 bp insertion and 3 bp deletion), we used the TFBSTools R package, as recommended by JASPAR. This package scans genomic sequences for TF binding sites based on PPMs, assigning each putative site a relative score between 0 and 1. We first analyzed the WT sequence, then introduced the mutations and rescanned each sequence.

Since the choice of score threshold significantly impacts TFBS predictions, we adopted an adaptive approach to ensure optimal sensitivity and specificity. While commonly used thresholds range from 0.75 to 0.9, we observed that each PPM exhibited a distinct score distribution across accessible genomic regions. To account for this variability, we tailored the threshold for each TF individually. We first applied TFBSTools to all accessible regions identified by ATAC-seq in mouse embryonic gonads at relevant developmental stages[45], using an initial threshold of 0.5. For each PPM, we identified the score cutoff corresponding to the top 1-5% of binding predictions. We then refined this by using known TFBS in Enh13 as a control, selecting the threshold that detected all known binding sites while minimizing the noise. The chosen thresholds were those that identified the top 2% of results. This

approach yielded an average threshold of 0.79, aligning with commonly used values. Finally, for each variant, we retained only TFBS predictions that exceeded the selected threshold in either the WT or mutated sequence.

Electromobility shift assay (EMSA)

Expression Plasmids with the T7 promoter were previously described for pcDNA3 human SOX9 and pcDNA3 human NR5A1[72]. Plasmid pcDNA3 mouse RUNX1 was obtained from Addgene (REF#14585). Plasmid pCS2^{+}mGATA4 was previously described[10] and originally obtained by FP from Dr. Sergei Tevosian. Proteins were produced using the TNT^{TM} coupled translation system (Promega) using T7 RNA polymerase for SOX9, RUNX1, NR5A1 and SP6 RNA polymerase for GATA4, according to the manufacturer's instructions. Negative control was programed with pLuciferase control vector from the TNT Kit. Probes were annealed by mixing 10 μg of each complementary oligonucleotide and heating at 95 °C for three minutes, then at Tm+5° for 5 min in 20 mM Tris pH 7.5, 5 mM NaCl, 1 mM EDTA, slow-cooled to 37 °C for 60 minutes and cooled to room-temperature. After annealing, the DNA duplexes were de-salted through a Sephadex G-50 spin column (GE healthcare, 27-5330-01). For radioactive labelling, a 5′ overhang G at both ends of probes was used to fill in with a[^{32}P]-dCTP (Amersham) using Superscript IV reverse transcriptase (Invitrogen). 100 ng of hybridized probes were incubated with 10μCi of dCTP and 1 μl of Superscript IV for 1 h at 37 °C in 1x RT buffer from the manufacturer. Un-incorporated nucleotides were removed through a Sephadex G-50 spin column. DNA binding assay was performed in a final volume of 20 μl with 10 mM Tris pH8, 100 mM KCl, 5 mM $MgCl_2$, 10 mM $ZnSO_4$, 1 mM Spermidine, 0.075% triton X100, 1 μg BSA, 1 mM DTT, 10% glycerol and 2 μl of in vitro translation mix. As non-specific competitors, for SOX9, 1 μg of poly dG-dC and for NR5A1, GATA4 and RUNX1, 0.1 μg of sonicated salmon sperm DNA were added. 0.5 ng of radio-labeled probe was added, binding reactions were performed on ice for 30 minutes and complexes were resolved on a 5% native acrylamide (37.5:1) gel in 0.5X Tris acetate buffer (10X: 400 mM Tris buffered to pH 7.8 with glacial acetic acid) at 4 °C, then dried and revealed using Molecular Dynamics PhosphoImager. Quantifications were performed using ImageQuant software. Statistics were performed using GraphPad Prism 9 with Ordinary one-way ANOVA with Tukey's multiple comparisons test.

Sequences of oligos for short probes

SOX9BS Enh13 Wt fw: gGGCTTGGGCAAGCAAACCACAACAATGGTC AGACTGATAA SOX9 BS Enh13 Wt rev: gTTATCAGTCTGAC-CATTGTTGTGGTTTGCTTGCCCAAGCCSOX9BS_mut_fw: gGGCTTG GGCAAGCAAACCAGGGGGGGGGTCAGACTGATAASOX9BS_mut_rev: gTTATCAGTCTGACCCCCCCCCTGGTTTGCTTGCCCAAGCCSOX9 BS del3bp fw: gGGCTTGGGCAAGCAAACCACAATGGTCAGACTGATAA-SOX9 BS del3bp rev: gTTATCAGTCTGACCATTGTGGTTTGC TTGCCCAAGCCSOX9 BS ins1bp fw: gGGCTTGGGCAAGCAAACCA-CAACAATGGTCAGACTGATAASOX9 BS ins1bp rev: gTTATCAG TCTGACCATTGTTGTGGTTTGCTTGCCCAAGCC

Sequences of oligos for long probes

Enh13-110-175-WT fw: gTGAGGAATTAGAAGGCCAGGTTGGCTTGGG CAAGCAAACCACAACAATGGTCAGACTGATAAAGCCCEnh13-110-175-WT rev:gGGCTTTATCAGTCTGACCATTGTTGTGGTTTGCTTGCCCAA GCCAACCTGGCCTTCTAATTCCTCAEnh13-110-175-del3bp fw:gTGA GGAATTAGAAGGCCAGGTTGGCTTGGGCAAGCAAACCACAATGGTC AGACTGATAAAGCCCEnh13-110-175-del3bp rev:gGGGCTTTATCAGT CTGACCATTGTGGTTTGCTTGCCCAAGCCAACCTGGCCTTCTAATTC CTCAEnh13-110-175-ins1bp fw:gTGAGGAATTAGAAGGCCAGGTTGGC TTGGGCAAGCAAACCACAATCAATGGTCAGACTGATAAAGCCEnh13-110-175-ins1bp rev:gGGCTTTATCAGTCTGACCATTGATTGTGGTTTG CTTGCCCAAGCCAACCTGGCCTTCTAATTCCTCA

Statistics & reproducibility

No formal statistical method was used to predetermine sample sizes. Instead, sample sizes were selected based on common practice for comparable assays and on ensuring reproducibility across independent experiments. All key experiments were performed with a minimum of three independent biological replicates. When increased variability was observed between replicates, additional independent repeats were performed to confirm results. Technical replicates where used, are indicated in the Methods/figure legends. Exact n values and what n represents are provided in each figure legend. Statistics were performed using GraphPad Prism 9 with either Ordinary two-way ANOVA or Ordinary one-way ANOVA with Tukey's multiple comparisons test, as stated in the figure legends.

Reporting summary

Further information on research design is available in the Nature Portfolio Reporting Summary linked to this article.

Data availability

All data is available in the manuscript or the supplementary materials. RNA-seq data and PBM data have been deposited in the Gene Expression Omnibus under accession numbers GSE291809 and GSE298334. Source data are provided with this paper.

Code availability

The code produced to analyze the data is available on GitHub: https://github.com/Istevant/Enh13_mutations.

References

1. Poulat, F. Non-Coding Genome, Transcription Factors, and Sex Determination. *Sex. Dev.* **15**, 295–307 (2021).
2. Stevant, I. & Nef, S. Genetic Control of Gonadal Sex Determination and Development. *Trends Genet.* **35**, 346–358 (2019).
3. Wilhelm, D., Palmer, S. & Koopman, P. Sex determination and gonadal development in mammals. *Physiol. Rev.* **87**, 1–28 (2007).
4. Zhao, F. & Yao, H. H. A tale of two tracts: history, current advances, and future directions of research on sexual differentiation of reproductive tracts. *Biol. Reprod.* **101**, 602–616 (2019).
5. Gonen, N. & Lovell-Badge, R. The regulation of Sox9 expression in the gonad. *Curr. Top. Dev. Biol.* **134**, 223–252 (2019).
6. Koopman, P., Gubbay, J., Vivian, N., Goodfellow, P. & Lovell-Badge, R. Male development of chromosomally female mice transgenic for Sry. *Nature* **351**, 117–121 (1991).
7. Sekido, R. & Lovell-Badge, R. Sex determination involves synergistic action of SRY and SF1 on a specific Sox9 enhancer. *Nature* **453**, 930–934 (2008).
8. Sinclair, A. H. et al. A gene from the human sex-determining region encodes a protein with homology to a conserved DNA-binding motif. *Nature* **346**, 240–244 (1990).
9. Koopman, P., Munsterberg, A., Capel, B., Vivian, N. & Lovell-Badge, R. Expression of a candidate sex-determining gene during mouse testis differentiation. *Nature* **348**, 450–452 (1990).
10. Rahmoun, M. et al. In mammalian foetal testes, SOX9 regulates expression of its target genes by binding to genomic regions with conserved signatures. *Nucleic Acids Res*, (2017).
11. Chaboissier, M. C. et al. Functional analysis of Sox8 and Sox9 during sex determination in the mouse. *Development* **131**, 1891–1901 (2004).
12. Foster, J. W. et al. Campomelic dysplasia and autosomal sex reversal caused by mutations in an SRY-related gene. *Nature* **372**, 525–530 (1994).
13. Koopman, P., Sinclair, A. & Lovell-Badge, R. Of sex and determination: marking 25 years of Randy, the sex-reversed mouse. *Development* **143**, 1633–1637 (2016).

14. Lavery, R. et al. XY Sox9 embryonic loss-of-function mouse mutants show complete sex reversal and produce partially fertile XY oocytes. *Dev. Biol.* **354**, 111–122 (2011).
15. Wagner, T. et al. Autosomal sex reversal and campomelic dysplasia are caused by mutations in and around the SRY-related gene SOX9. *Cell* **79**, 1111–1120 (1994).
16. Huang, B., Wang, S., Ning, Y., Lamb, A. N. & Bartley, J. Autosomal XX sex reversal caused by duplication of SOX9. *Am. J. Med Genet* **87**, 349–353 (1999).
17. Vidal, V. P., Chaboissier, M. C., de Rooij, D. G. & Schedl, A. Sox9 induces testis development in XX transgenic mice. *Nat. Genet.* **28**, 216–217 (2001).
18. Bishop, C. E. et al. A transgenic insertion upstream of sox9 is associated with dominant XX sex reversal in the mouse. *Nat. Genet.* **26**, 490–494 (2000).
19. Qin, Y. et al. Long-range activation of Sox9 in Odd Sex (Ods) mice. *Hum. Mol. Genet.* **13**, 1213–1218 (2004).
20. Gregoire, E. P. et al. The -KTS splice variant of WT1 is essential for ovarian determination in mice. *Science* **382**, 600–606 (2023).
21. Chassot, A. A. et al. WNT4 and RSPO1 together are required for cell proliferation in the early mouse gonad. *Development* **139**, 4461–4472 (2012).
22. Chassot, A. A. et al. Activation of beta-catenin signaling by Rspo1 controls differentiation of the mammalian ovary. *Hum. Mol. Genet.* **17**, 1264–1277 (2008).
23. Maatouk, D. M., Mork, L., Chassot, A. A., Chaboissier, M. C. & Capel, B. Disruption of mitotic arrest precedes precocious differentiation and transdifferentiation of pregranulosa cells in the perinatal Wnt4 mutant ovary. *Dev. Biol.* **383**, 295–306 (2013).
24. Tomizuka, K. et al. R-spondin1 plays an essential role in ovarian development through positively regulating Wnt-4 signaling. *Hum. Mol. Genet.* **17**, 1278–1291 (2008).
25. Vainio, S., Heikkila, M., Kispert, A., Chin, N. & McMahon, A. P. Female development in mammals is regulated by Wnt-4 signalling. *Nature* **397**, 405–409 (1999).
26. Ottolenghi, C. et al. Foxl2 is required for commitment to ovary differentiation. *Hum. Mol. Genet.* **14**, 2053–2062 (2005).
27. Schmidt, D. et al. The murine winged-helix transcription factor Foxl2 is required for granulosa cell differentiation and ovary maintenance. *Development* **131**, 933–942 (2004).
28. Uhlenhaut, N. H. et al. Somatic sex reprogramming of adult ovaries to testes by FOXL2 ablation. *Cell* **139**, 1130–1142 (2009).
29. Nicol, B. et al. RUNX1 maintains the identity of the fetal ovary through an interplay with FOXL2. *Nat. Commun.* **10**, 5116 (2019).
30. Auguste, A. et al. Loss of R-spondin1 and Foxl2 amplifies female-to-male sex reversal in XX mice. *Sex. Dev.* **5**, 304–317 (2011).
31. Ottolenghi, C. et al. Loss of Wnt4 and Foxl2 leads to female-to-male sex reversal extending to germ cells. *Hum. Mol. Genet.* **16**, 2795–2804 (2007).
32. Wilhelm D., Perea-Gomez A., Newton A., Chaboissier M. C. Gonadal sex determination in vertebrates: rethinking established mechanisms. *Development* **152**, (2025).
33. Biason-Lauber, A. & Chaboissier, M. C. Ovarian development and disease: The known and the unexpected. *Semin Cell Dev. Biol.* **45**, 59–67 (2015).
34. Gonen, N. et al. Sex reversal following deletion of a single distal enhancer of Sox9. *Science* **360**, 1469–1473 (2018).
35. Ogawa, Y. et al. Mapping of a responsible region for sex reversal upstream of Sox9 by production of mice with serial deletion in a genomic locus. *Sci. Rep.* **8**, 17514 (2018).
36. Ridnik, M. et al. Two redundant transcription factor binding sites in a single enhancer are essential for mammalian sex determination. *Nucleic Acids Res.* **52**, 5514–5528 (2024).
37. Croft, B. et al. Human sex reversal is caused by duplication or deletion of core enhancers upstream of SOX9. *Nat. Commun.* **9**, 5319 (2018).
38. Sajan, S. A. et al. The smallest likely pathogenic duplication of a SOX9 enhancer identified to date in a family with 46, XX testicular differences of sex development. *Am. J. Med. Genet. A*, (2023).
39. Burgoyne, P. S. The role of the mammalian Y chromosome in spermatogenesis. *Development* **101**, 133–141 (1987).
40. da Silva, M. orais et al. R. Sox9 expression during gonadal development implies a conserved role for the gene in testis differentiation in mammals and birds. *Nat. Genet.* **14**, 62–68 (1996).
41. Zhao, L. et al. Transcriptomic analysis of mRNA expression and alternative splicing during mouse sex determination. *Mol Cell Endocrinol*, (2018).
42. Colvin, J. S., Green, R. P., Schmahl, J., Capel, B. & Ornitz, D. M. Male-to-female sex reversal in mice lacking fibroblast growth factor 9. *Cell* **104**, 875–889 (2001).
43. Stevant, I. et al. The gene regulatory landscape driving mouse gonadal supporting cell differentiation. *Sci. Adv.* **11**, eadv1885 (2025).
44. Mayere, C. et al. Origin, specification and differentiation of a rare supporting-like lineage in the developing mouse gonad. *Sci. Adv.* **8**, eabm0972 (2022).
45. Stévant I. et al. Divergent regulatory element programs steer sex-specific supporting cell differentiation along mouse gonadal development. *bioRxiv*, 2024.2012.2009.627451 (2024).
46. Stevant, I. et al. Dissecting Cell Lineage Specification And Sex Fate Determination In Gonadal Somatic Cells Using Single-cell Transcriptomics. *Cell Rep.* **26**, 3272–3283.e3273 (2019).
47. de Santa Barbara, P., Moniot, B., Poulat, F. & Berta, P. Expression and subcellular localization of SF-1, SOX9, WT1, and AMH proteins during early human testicular development. *Dev. Dyn.* **217**, 293–298 (2000).
48. Berger, M. F. & Bulyk, M. L. Protein binding microarrays (PBMs) for rapid, high-throughput characterization of the sequence specificities of DNA binding proteins. *Methods Mol. Biol.* **338**, 245–260 (2006).
49. Spitz, F. & Furlong, E. E. Transcription factors: from enhancer binding to developmental control. *Nat. Rev. Genet.* **13**, 613–626 (2012).
50. Kim, S. et al. DNA-guided transcription factor cooperativity shapes face and limb mesenchyme. *Cell* **187**, 692–711.e626 (2024).
51. Ambrosetti, D. C., Basilico, C. & Dailey, L. Synergistic activation of the fibroblast growth factor 4 enhancer by Sox2 and Oct-3 depends on protein-protein interactions facilitated by a specific spatial arrangement of factor binding sites. *Mol. Cell Biol.* **17**, 6321–6329 (1997).
52. Merika, M. & Orkin, S. H. DNA-binding specificity of GATA family transcription factors. *Mol. Cell Biol.* **13**, 3999–4010 (1993).
53. Shimizu, S. et al. Multimerization of the GATA4 transcription factor regulates transcriptional activity and cardiomyocyte hypertrophic response. *Int J. Biol. Sci.* **18**, 1079–1095 (2022).
54. Ogawa, Y. et al. SOX9 and SRY binding sites on mouse mXYSRa/Enh13 enhancer redundantly regulate Sox9 expression to varying degrees. *Hum. Mol. Genet.* **32**, 55–64 (2023).
55. Ogawa, Y. et al. Author Correction: GATA4 binding to the Sox9 enhancer mXYSRa/Enh13 is critical for testis differentiation in mouse. *Commun. Biol.* **8**, 199 (2025).
56. Rousseau, S. et al. A genome-wide association study points out the causal implication of SOX9 in the sex-reversal phenotype in XX pigs. *PLoS One* **8**, e79882 (2013).
57. Gasca, S. et al. A nuclear export signal within the high mobility group domain regulates the nucleocytoplasmic translocation of SOX9 during sexual determination. *Proc. Natl. Acad. Sci. USA* **99**, 11199–11204 (2002).

58. Xu, G. et al. Physical association of the patient-specific GATA1 mutants with RUNX1 in acute megakaryoblastic leukemia accompanying Down syndrome. *Leukemia* **20**, 1002–1008 (2006).
59. Ferjoux, G., Auge, B., Boyer, K., Haenlin, M. & Waltzer, L. A GATA/RUNX cis-regulatory module couples Drosophila blood cell commitment and differentiation into crystal cells. *Dev. Biol.* **305**, 726–734 (2007).
60. Jindal, G. A. & Farley, E. K. Enhancer grammar in development, evolution, and disease: dependencies and interplay. *Dev. Cell* **56**, 575–587 (2021).
61. Lim, F. et al. Affinity-optimizing enhancer variants disrupt development. *Nature* **626**, 151–159 (2024).
62. Xie, Z. et al. DNA-guided transcription factor interactions extend human gene regulatory code. *Nature* **641**, 1329–1338 (2025).
63. Dodonova, S. O., Zhu, F., Dienemann, C., Taipale, J. & Cramer, P. Nucleosome-bound SOX2 and SOX11 structures elucidate pioneer factor function. *Nature* **580**, 669–672 (2020).
64. Fuglerud, B. M. et al. SOX9 reprograms endothelial cells by altering the chromatin landscape. *Nucleic Acids Res.* **50**, 8547–8565 (2022).
65. Hojo, H. & Ohba, S. Runt-related Transcription Factors and Gene Regulatory Mechanisms in Skeletal Development and Diseases. *Curr. Osteoporos. Rep.* **21**, 485–492 (2023).
66. Barral, A. & Zaret, K. S. Pioneer factors: roles and their regulation in development. *Trends Genet.* **40**, 134–148 (2024).
67. Cirillo, L. A. et al. Opening of compacted chromatin by early developmental transcription factors HNF3 (FoxA) and GATA-4. *Mol. Cell* **9**, 279–289 (2002).
68. Sudbeck, P., Schmitz, M. L., Baeuerle, P. A. & Scherer, G. Sex reversal by loss of the C-terminal transactivation domain of human SOX9. *Nat. Genet.* **13**, 230–232 (1996).
69. Shifera, A. S. & Hardin, J. A. Factors modulating expression of Renilla luciferase from control plasmids used in luciferase reporter gene assays. *Anal. Biochem.* **396**, 167–172 (2010).
70. Berger, M. F. et al. Compact, universal DNA microarrays to comprehensively determine transcription-factor binding site specificities. *Nat. Biotechnol.* **24**, 1429–1435 (2006).
71. Berger, M. F. & Bulyk, M. L. Universal protein-binding microarrays for the comprehensive characterization of the DNA-binding specificities of transcription factors. *Nat. Protoc.* **4**, 393–411 (2009).
72. De Santa Barbara, P. et al. Direct interaction of SRY-related protein SOX9 and steroidogenic factor 1 regulates transcription of the human anti-Mullerian hormone gene. *Mol. Cell Biol.* **18**, 6653–6665 (1998).

Acknowledgements

We thank the BIU animal facility and technicians for their help with animal maintenance. We are grateful to the BIU transgenic facility for the production of CRISPR genome-edited mice. We acknowledge the Life Sciences Microscopy unit at BIU for help with imaging. This work is co-funded by the Israel Science Foundation (ISF_710_2020, ISF_976_25) and the European Union (ERC, *EnhanceSex*, 101039928). Views and opinions expressed are, however, those of the authors only and do not necessarily reflect those of the European Union or the European Research Council. Neither the European Union nor the granting authority can be held responsible for them. FP was funded by ANR-23-CE14-0012-01 (Heterosex). Ariel Afek was funded by the Israel Science Foundation (ISF_1174_2022).

Author contributions

E.A. and N.G. conceived the experiments; E.A., M.R. performed experiments and analysed the data. C.B. helped with mice colony management and genotyping. R.W. performed the JASPAR analysis. Y.M.Y. and A.A. performed the PBM assays, I.S. analysed the RNA-seq and the PBM data. S.Z.L. and M.L. generated the CRISPR-genome edited mice. F.P. performed and analysed the EMSA experiments. The manuscript was written by N.G., E.A. and F.P. All authors read and accepted the data being presented in the manuscript.

Competing interests

The authors declare no competing interests.

Additional information

Supplementary information The online version contains supplementary material available at https://doi.org/10.1038/s41467-026-71328-9.

Correspondence and requests for materials should be addressed to Nitzan Gonen.

Peer review information *Nature Communications* thanks Eric Pailhoux and the other anonymous reviewer(s) for their contribution to the peer review of this work. A peer review file is available.

Reprints and permissions information is available at http://www.nature.com/reprints

Publisher's note Springer Nature remains neutral with regard to jurisdictional claims in published maps and institutional affiliations.

Open Access This article is licensed under a Creative Commons Attribution-NonCommercial-NoDerivatives 4.0 International License, which permits any non-commercial use, sharing, distribution and reproduction in any medium or format, as long as you give appropriate credit to the original author(s) and the source, provide a link to the Creative Commons licence, and indicate if you modified the licensed material. You do not have permission under this licence to share adapted material derived from this article or parts of it. The images or other third party material in this article are included in the article's Creative Commons licence, unless indicated otherwise in a credit line to the material. If material is not included in the article's Creative Commons licence and your intended use is not permitted by statutory regulation or exceeds the permitted use, you will need to obtain permission directly from the copyright holder. To view a copy of this licence, visit http://creativecommons.org/licenses/by-nc-nd/4.0/.

© The Author(s) 2026